View metadata, citation and similar papers at core.ac.uk
brought to you by CORE
provided by University of Queensland eSpace

PHYSICAL REVIEW B **73**, 235107 (2006)

Ferromagnetism, paramagnetism, and a Curie-Weiss metal in an electron-doped Hubbard model on a triangular lattice

J. Merino,[1] B. J. Powell,[2] and Ross H. McKenzie[2]
[1]*Departamento de Física Teórica de la Materia Condensada, Universidad Autónoma de Madrid, Madrid 28049, Spain*
[2]*Department of Physics, University of Queensland, Brisbane, Qld 4072, Australia*
(Received 4 January 2006; revised manuscript received 27 April 2006; published 8 June 2006)

Motivated by the unconventional properties and rich phase diagram of Na_xCoO_2 we consider the electronic and magnetic properties of a two-dimensional Hubbard model on an isotropic triangular lattice doped with electrons away from half-filling. Dynamical mean-field theory (DMFT) calculations predict that for negative intersite hopping amplitudes ($t<0$) and an on-site Coulomb repulsion, U, comparable to the bandwidth, the system displays properties typical of a weakly correlated metal. In contrast, for $t>0$ a large enhancement of the effective mass, itinerant ferromagnetism, and a metallic phase with a Curie-Weiss magnetic susceptibility are found in a broad electron doping range. The different behavior encountered is a consequence of the larger noninteracting density of states (DOS) at the Fermi level for $t>0$ than for $t<0$, which effectively enhances the mass and the scattering amplitude of the quasiparticles. The shape of the DOS is crucial for the occurrence of ferromagnetism as for $t>0$ the energy cost of polarizing the system is much smaller than for $t<0$. Our observation of Nagaoka ferromagnetism is consistent with the A-type antiferromagnetism (i.e., ferromagnetic layers stacked antiferromagnetically) observed in neutron scattering experiments on Na_xCoO_2. The transport and magnetic properties measured in Na_xCoO_2 are consistent with DMFT predictions of a metal close to the Mott insulator and we discuss the role of Na ordering in driving the system towards the Mott transition. We propose that the "Curie-Weiss metal" phase observed in Na_xCoO_2 is a consequence of the crossover from a "bad metal" with incoherent quasiparticles at temperatures $T>T^*$ and Fermi liquid behavior with enhanced parameters below T^*, where T^* is a low energy coherence scale induced by strong local Coulomb electron correlations. Our analysis also shows that the one band Hubbard model on a triangular lattice is not enough to describe the unusual properties of Na_xCoO_2 and is used to identify the simplest relevant model that captures the essential physics in Na_xCoO_2. We propose a model which allows for the Na ordering phenomena observed in the system which, we propose, drives the system close to the Mott insulating phase even at large dopings.

DOI: 10.1103/PhysRevB.73.235107 PACS number(s): 71.10.Hf, 71.30.+h

I. INTRODUCTION

One of the outstanding problems in quantum many-body physics is to understand quasi-two-dimensional systems in which both electron-electron interactions and frustration effects are strong.[1] New exotic phases are expected to result from the interplay of these effects. Recently a number of materials have been discovered where the interplay of geometrical frustration and strong electronic correlations lead to the emergence of unconventional phases. Examples of such materials include inorganic materials and organic charge transfer salts such as κ-(BEDT-TTF)$_2$Cu$_2$(CN)$_3$ or β'-[Pd(dmit)$_2$]X (Refs. 2 and 3 explain this nomenclature). Antiferromagnets on triangular lattices may be isotropic as in $NiGa_2S_4$, κ-(BEDT-TTF)$_2$Cu$_2$(CN)$_3$ and, the material we will focus on, Na_xCoO_2, or anisotropic as in Cs_2CuCl_4, κ-(BEDT-TTF)$_2$Cu[N(CN)$_2$]Cl. There is also a great deal of interest in other frustrated geometries such as the Kagome and pyrochlore lattices. However, Na_xCoO_2 has the, so far, unique property among strongly correlated triangular lattice compounds, that it can be doped. In κ-(ET)$_2$Cu$_2$(CN)$_3$ a spin liquid state gives way to superconductivity when hydrostatic pressure is applied.[4] The β'-[Pd(dmit)$_2$]X series[5] of compounds, Cs_2CuCl_4 (Ref. 6) and $NiGa_2S_4$ (Ref. 7) may also show spin liquid behavior. Interestingly, the underlying structures of κ-(ET)$_2$Cu$_2$(CN)$_3$ and the β'-[Pd(dmit)$_2$]X compounds are very similar to that of $NiGa_2S_4$ and Na_xCoO_2 with either the organic molecules, the Ni atoms or the Co atoms arranged in a triangular geometry. Understanding the physics of these systems in which both frustration and correlations are present is clearly a major challenge to theory.

Much attention has been focused on the occurrence of superconductivity in $Na_xCoO_2\cdot yH_2O$. However, the nonsuperconducting, nonhydrated counterpart, Na_xCoO_2, displays many interesting magnetic and electronic properties. These include a charge ordered insulating state in a narrow band of doping around[8] $x=0.5$, A-type antiferromagnetism[9] for $x \gtrsim 0.75$ and a metallic phase with a Curie-Weiss susceptibility, $\chi(T)\sim 1/(T+\theta)$, whose magnitude is much larger than the Pauli susceptibility expected for a weakly interacting metal[8] (the Curie-Weiss metal). This phase also has an extremely large thermopower (of order k_B/e) that is temperature and field dependent.[10] Foo *et al.* suggested[8] that the metallic state for $x<0.5$ should be regarded as paramagnetic and the state for $0.5<x<0.75$ be thought of as a Curie-Weiss metal. These results should be compared with the measurements of Prabhakaran *et al.*[11] which display a different behavior with the Curie-Weiss behavior that is strongest at $x=0.5$ (the lowest value of x in their sample set) and the susceptibility becoming less temperature dependent as x is increased. These differences may be due to the rather different strength fields used in the two different experiments,[12] a strong dependence on the direction of the field or to some extrinsic effect. For $x>0.75$ A-type antiferromagnetism (in-

 ©2006 The American Physical Society

plane ferromagnetic ordering stacked in alternate directions along the c axis) is observed.[13–16] On the triangular lattice this raises the interesting possibility of in-plane Nagaoka ferromagnetism,[17] which we will discuss further below. There is also direct experimental evidence for strong electron-electron correlations which comes from unconventional behavior of transport properties. For instance, a Fermi liquid like resistivity $[\rho(T)=\rho_0+AT^2]$ is only observed[18] for $T\lesssim 1$ K, and the value of the Kadowaki-Woods ratio is comparable to ruthenates and heavy fermions.[18,19] The low temperature scale and the Kadowaki-Woods ratio are strongly field dependent with the system becoming more weakly correlated with increasing field.

Interestingly, some of the above properties are reminiscent of the predictions of the dynamical mean-field theory (DMFT) of the Hubbard model.[20] At half filling $(n=1)$ DMFT predicts a Mott metal-insulator transition for $U\sim W$. In the metallic phase close to the Mott transition there is a low temperature scale, $T^*(n)$, at which there is a smooth crossover from a Fermi liquid to an incoherent "bad metal."[20–22] Transport properties display a crossover from those expected in a Fermi liquid to properties characteristic of incoherent excitations as the temperature is increased. Within the "bad metal" phase, that is for $T>T^*$, electrons behave as quasilocalized moments which leads to a Curie-Weiss behavior of the magnetic susceptibility.[20,21] The above discussion suggests that DMFT, which treats the local electronic correlations exactly, may capture the relevant physics needed to describe the temperature dependence of many of the transport and magnetic properties of Na_xCoO_2.

An important first step in studying the properties of Na_xCoO_2 is to consider the two-dimensional triangular lattice Hubbard model. This is motivated by the arrangement of the Co atoms and because correlation effects can be singled out and better understood in the simplest model. Related models such as the t-J model on the triangular lattice have been recently analyzed using resonating valence bond (RVB) theory.[23] The implicit assumption in this kind of approach is that many important aspects of more realistic models for Na_xCoO_2 are already contained in the simpler triangular lattice model. Our present study, however, leads to the important conclusion that a single band Hubbard model on a triangular lattice is not enough to describe the magnetic and electronic properties of Na_xCoO_2 and a more realistic model is proposed.

Our main finding, summarized in Fig. 1, is that DMFT predicts dramatic changes in the behavior of the Hubbard model on a triangular lattice when the sign of t is changed. For $t>0$ we find significant effects due to strong electronic correlations. We find that in the electron doped triangular lattice a Curie-Weiss metal and metallic ferromagnetism arise when only local Coulomb correlations are taken into account. The Curie-Weiss metal occurs for sufficiently large Coulomb repulsion energies $U\gtrsim W$ and $t>0$, where W is the bandwidth. In this parameter region, the local magnetic susceptibility smoothly changes from the Curie form characteristic of local moments at high temperature to Fermi liquid behavior at low temperatures, $T<T^*(n)\ll\epsilon_F$, where ϵ_F is the Fermi energy. In the Curie-Weiss metal the uniform susceptibility is strongly enhanced by both band narrowing due to

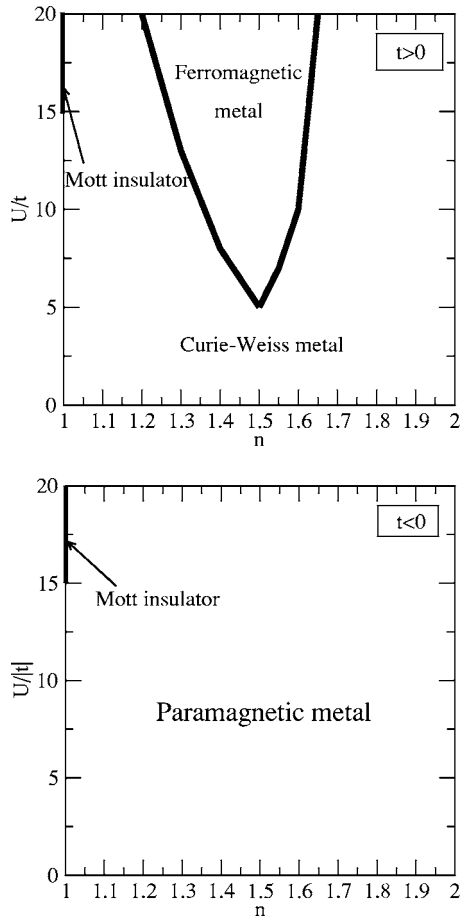

FIG. 1. Phase diagram for the electron doped Hubbard model on a triangular lattice obtained from DMFT calculations. $U/|t|$ is the ratio of the on-site Coulomb repulsion to the absolute value of the hopping matrix element t and n is the average number of electrons per site. The sign of t leads to qualitative changes in the phase diagram. In the $t>0$ case, a ferromagnetic metal and a metal with Curie-Weiss susceptibility are found. In contrast, for $t<0$ a paramagnetic metal appears throughout the phase diagram. To make a direct comparison with Na_xCoO_2 one should note that $x=n-1$.

correlations and the proximity to the ferromagnetic instability. In contrast, the electron doped triangular Hubbard model with $t<0$ and $U\gtrsim W$ displays Pauli paramagnetism weakly enhanced by the Coulomb repulsion; a behavior typical of weakly correlated metals. Thus our analysis shows how the noninteracting dispersion has a dramatic effect on the electronic and magnetic properties of a frustrated Hubbard model. Thus, our work is relevant to DMFT applications on real materials where similar LDA density of states appear to help in understanding the physics in the more complicated situations.

The remainder of this paper is organized as follows: In Sec. II we introduce the Hubbard model on a triangular model discussed above, and then examine the solution of this model on three sites which already contains some features of, and gives significant insight to, the solution of the triangular lattice in the thermodynamic limit. In Sec. III we introduce the main DMFT equations and present arguments which suggest that DMFT, which is only exact in infinite dimensions,

may capture the essential physics of the Hubbard model on a two-dimensional triangular lattice due to frustration. In Sec. IV we analyze the temperature dependence of the local and uniform magnetic susceptibilities for both $t<0$ and $t>0$. In Sec. V we analyze the local correlation effects and the electronic properties of the model. We report spectral densities and self-energies in both signs of t and their relation with the different magnetic susceptibilities found in Sec. IV. In Sec. VI we show that for $t>0$ and electron doping we find Nagaoka ferromagnetism. In Sec. VII we discuss the experimental situation on Na_xCoO_2 in the light of our results. In Sec. VIII we discuss improvements and extensions to both the model and the approximation used to study it, we argue that multiple band models and particularly the effects of ordering of the Na ions are essential to understand the behavior observed in Na_xCoO_2. The paper ends in Sec. IX in which a summary of main results is given and our conclusions are drawn.

II. THE HUBBARD MODEL ON A TRIANGULAR LATTICE

As stated in the Introduction, we analyze the magnetic and electronic properties of a Hubbard model on a triangular lattice,

$$H = -t\sum_{\langle ij\rangle,\sigma}(c^{\dagger}_{i\sigma}c_{j\sigma}+\text{H.c.}) + U\sum_{i} n_{i\uparrow}n_{i\downarrow} - \mu\sum_{i,\sigma} n_{i\sigma}, \quad (1)$$

where μ, t, and U are the chemical potential, the nearest-neighbor hopping amplitude, and the on-site Coulomb repulsion energies, respectively, $c^{(\dagger)}_{i\sigma}$ (creates) destroys an electron on site i with spin σ, $\langle\cdots\rangle$ indicates that the sum is over nearest neighbors only and the number operator is $n_{i\sigma} \equiv c^{\dagger}_{i\sigma}c_{i\sigma}$.

For $U=0$ the above model gives a tight-binding dispersion

$$\epsilon_{\mathbf{k}} = -2t\cos(k_x) - 4t\cos\left(\frac{\sqrt{3}}{2}k_y\right)\cos\left(\frac{k_x}{2}\right) - \mu, \quad (2)$$

with bandwidth $W=9|t|$.

A. Review of previous work

For the Hubbard model on the square lattice at half filling, the ground state is believed to be a Mott insulator with Néel order for all values of U/t. The fact that this occurs even for arbitrarily small U/t is due to the perfect nesting of the noninteracting Fermi surface at half filling. In contrast, the triangular lattice may exhibit diverse phases as U/t is varied. Possible ground states that have been proposed include the Mott insulator, commensurate noncollinear antiferromagnetism, incommensurate spin-density wave (both metallic and insulating), spin liquid, superconducting, and metallic states.

In the strong correlation limit, $U \gg t$, there is a gap in the charge excitation spectrum and the ground state is a Mott insulator. The spin excitations are described by an antiferromagnetic Heisenberg model on the triangular lattice with exchange constant $J=4t^2/U$. Numerical calculations from a range of techniques including exact diagonalization,[24] variational quantum Monte Carlo,[25,26] coupled cluster methods,[27] and series expansions[28,29] suggest that this has a magnetically ordered ground state in which neighboring spins are rotated by 120° relative to one another, as in the classical ground state. This agrees with the predictions of spin wave theory.[30] However, series expansions calculations suggest that the excitation spectrum is qualitatively different from that predicted by nonlinear spin wave theory.[31]

At half-filling there is no nesting of the noninteracting Fermi surface and so for small U/t a metallic state is possible. Exact diagonalization calculations of the Drude weight for lattices with 12 sites suggest that there is a first-order transition from a metal to a Mott insulator when $U \simeq 12.1t$,[32] mean-field RVB calculations in the thermodynamic limit find a remarkably similar result with a first order Mott transition occurring at $U \simeq 12.4t$.[33] When $U \sim 4t$ the effective spin Hamiltonian in Mott insulating phase should include ring exchange terms of order t^3/U^2 (Ref. 34). On the triangular lattice this can lead to a spin liquid ground state.[35] The possible realization of a spin liquid in κ-$(ET)_2Cu_2(CN)_3$ (Ref. 4) has stimulated the proposal of specific analytical theories for the ground state in this regime.[36,37] In this parameter regime a superconducting ground state with $d+id$ symmetry,[38] or odd frequency pairing[39] have also been proposed [it is therefore interesting to note that odd frequency pairing has also been discussed on the basis of specific microscopic calculations for $Na_xCoO_2 \cdot yH_2O$ (Ref. 40)].

Hartree-Fock[41] and slave boson mean-field calculations[42] have found that near the metal-insulator phase boundary that incommensurate spin-density wave states are also stable. Simulated annealing calculations of mean-field solutions with large possible unit cells found that for $U=2t$ and $U=4t$ that the most stable states were metals with charge and spin ordering.[43]

For electron doping away from half-filling and $U \gg t$, doubly occupied states can be projected out and a t-J model can describe the system. Extensive studies of this model have been made.[23,44] These studies show that the sign of t has a significant effect on the type of ground state.[23] RVB calculations[23,44] found that, for $t>0$, $d+id$ superconductivity was possible for a range of dopings and suggested a variety of unusual metallic states. Series expansions[45] have emphasized the competition between singlet and triplet formation on the triangular lattice in terms of competition between RVB states and Nagaoka ferromagnetism. This work concludes that for hole doping the RVB state is favored by $t>0$ and the Nagaoka state is favored by $t<0$. Changing the sign of t is equivalent to changing from electron to hole doping, therefore this result is entirely consistent with the results summarized in Fig. 1. A more detailed comparison between our results and those of Koretsune and Ogata[45] will be given in Sec. VI.

B. Relevance to Na_xCoO_2

For Na_xCoO_2 the LDA bandwidth gives $|t| \sim 0.1$ eV.[47,48] For electron doping the dispersion (2) leads to a Fermi surface which is hole-like for $t<0$ and electron-like for $t>0$,

thus $t<0$ is roughly consistent with the band structure calculations and angle resolved photoemission spectroscopy (ARPES) experiments for Na_xCoO_2. However, the band structure of Na_xCoO_2 is still controversial. ARPES (Ref. 46) seems to suggest that a simple tight binding model with $t<0$ on the triangular lattice may be sufficient to describe the a_{1g} bands of Na_xCoO_2. However, even within a single band model hopping matrix elements up to at least third nearest neighbors[48–50] need to be included in order to correctly reproduce the LDA band structure. Further, LDA calculations[47,48] predict the existence of six small elliptical hole pockets near to the K points if $x \lesssim 0.6$. It is not clear, at this point, whether or not the elliptical pockets actually exist.[51,52] In contrast to the a_{1g} bands, the LDA dispersion of the e_{1g} bands is better fitted to a $t>0$ triangular lattice tight-binding dispersion.[48]

Several attempts[46,47] have been made to estimate U for Na_xCoO_2; all of these find that $U \gg W$. This is much larger than in the organic charge transfer salts such as κ-$(ET)_2Cu_2(CN)_3$ or β'-$[Pd(dmit)_2]X$, in which $U \gtrsim W$ (Ref. 53, and references therein).

It is worth keeping in mind the limitations of this Hamiltonian as a model for Na_xCoO_2. For instance, the charge ordered state observed in a narrow region around $x=0.5$ seems likely to be due to the response of the electronic system to the ordering of the Na atoms which is observed even at high temperatures by x-ray diffraction.[8] Therefore one does not expect this phase to appear in purely electronic models such as those considered here. Nevertheless, before attempting to understand more complicated models with realistic band structures (including possibly multiple bands) or including the effects of Na ordering, it is important to have a firm understanding of strong correlations in simple frustrated models. Therefore, despite the remarks above, we present below a DMFT study of the Hubbard model on a triangular lattice (1). In Sec. VIII B we discuss extensions to the Hubbard model which allow one to investigate such effects.

C. Kinetic energy frustration

Geometrically frustrated antiferromagnetism has been studied extensively and the triangular lattice provides a model system to investigate. Three of the most widely used quantitative measures of frustration in antiferromagnets are (i) the degeneracy of the ground state, (ii) the magnitude of the entropy at low temperatures, and (iii) the ratio of the ground state energy to the total energy of maximising the individual interaction energies.[31]

In a noninteracting electron model the only proposal we are aware of for a quantitative measure of the geometrical frustration of the kinetic energy is due to Barford and Kim.[54] They noted that, for $t>0$, an electron at the bottom of the band does not gain the full lattice kinetic energy, while a hole at the top of the band does. They suggested that for tight binding models a measure of the frustration is then $\Delta = |\epsilon_k^{\max}| - |\epsilon_k^{\min}|$, where $\epsilon_k^{\max}$ and $\epsilon_k^{\min}$ are the energies (relative to the energy of the system with no electrons) of the top and bottom of the band, respectively. This frustration increases the density of states for positive energies for $t>0$ (negative energies for $t<0$) which represents an increased degeneracy and enhances the many-body effects when the Fermi energy is in this regime. However, perhaps a simpler measure of the kinetic energy frustration is $W/2z|t|$, where W is the bandwidth and z is the coordination number of the lattice. The smaller this ratio, the stronger the frustration is, while for an unfrustrated lattice $W/2z|t|=1$. For example, on the triangular lattice the kinetic energy frustration leads to a bandwidth, $W=9|t|$, instead of $12|t|$ as one might naively predict from $W=2z|t|$ since $z=6$.

We show below that geometrical frustration of the kinetic energy is a key concept required to understand the properties of the Hubbard model on the triangular lattice. In particular it leads to particle-hole asymmetry which enhances many-body effects for electron (hole) doped $t>0$ ($t<0$) lattices.

It should be noted that geometrical frustration of the kinetic energy is a strictly quantum mechanical effect arising from quantum interference. This interference arises from hopping around triangular clusters which will have an amplitude proportional to t^3 which clearly changes sign when t changes sign. In contrast on the, unfrustrated, square lattice the smallest possible cluster is the square and the amplitude for hopping around a square is independent of the sign of t as it is proportional to t^4. Barford and Kim[54] noted that the phase collected by hopping around a frustrated cluster may be exactly canceled by the Aharonov-Bohm phase associated with hopping around the cluster for a particular choice of applied magnetic field. Thus a magnetic field may be used to lift the effects of kinetic energy frustration. The quantum mechanical nature of kinetic energy frustration is in distinct contrast to geometrical frustration in antiferromagnets which can occur for purely classical spins.

D. The Hubbard model on a triangular cluster

1. Noninteracting case ($U=0$)

In order to gain some basic insights into some of the rich physics associated with the triangular lattice Hubbard model, we now review the exact solution on a single triangle. This is the simplest possible model with kinetic frustration and strongly correlated electrons. This model already contains some of the features found in the solution of the Hubbard model on the triangular lattice in the thermodynamic limit and gives significant insight into that problem. In particular the solution of this toy problem illustrates why the sign of t is important and why ferromagnetism arises in the solution to a problem that only contains kinetic, local and (via superexchange) antiferromagnetic interactions.

Let us begin by recalling the solution of the two site cluster with $U=0$ and spinless fermions. Let us label the Wannier functions on the two sites $|1\rangle$ and $|2\rangle$. For $t>0$ the single electron ground state is the bonding orbital with wave function $|\Psi\rangle = \frac{1}{\sqrt{2}}(|1\rangle + |2\rangle)$ and energy $E=-t=-|t|$. For $t<0$ the single electron ground state is the antibonding orbital with $|\Psi\rangle = \frac{1}{\sqrt{2}}(|1\rangle - |2\rangle)$ and $E=t=-|t|$. (Note that in general changing the sign of t reverses the ordering of the energy levels.) Thus $W=2t$ for the two site cluster which, as $z=1$ for the two site lattice, fits with the general expectation that, for an un-

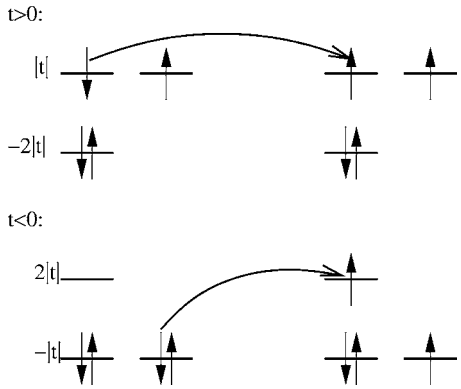

FIG. 2. Energy cost in spin polarizing the three site triangular cluster with four noninteracting electrons. For $t>0$ the ground state is degenerate and there is no energy cost in flipping one spin. In contrast, it costs $3|t|$ to polarize the $t<0$ cluster. This indicates that the tendency to ferromagnetism of the electron doped $t>0$ triangular cluster is much stronger than that of the cluster with $t<0$ even at the one-electron level.

frustrated lattice, the bandwidth is given by $2zt$.

The ground state of the $U=0$ triangular cluster has some significantly different properties compared to the two-site cluster. For $t>0$ the single electron ground state is completely bonding with $|\Psi\rangle=\frac{1}{\sqrt{3}}(|1\rangle+|2\rangle+|3\rangle)$ and $E=-2t=-2|t|$, but for $t<0$ we cannot construct a completely antibonding solution and so the single electron ground state is degenerate with $|\Psi\rangle=\frac{1}{\sqrt{6}}(|1\rangle-2|2\rangle+|3\rangle)$ or $|\Psi\rangle=\frac{1}{\sqrt{6}}(|1\rangle+|2\rangle-2|3\rangle)$ and $E=t=-|t|$. Thus even at the noninteracting level the bandwidth is reduced ($W=3t$, $z=2$ which implies $W/2zt=3/4$) by the effects of geometric frustration.

Moving to noninteracting spin 1/2 fermions, one can already see how the three site cluster with $t>0$ is easier to magnetize than the $t<0$ case. In Fig. 2 the energy level structure of the $t<0$ and $t>0$ three site clusters containing four electrons are displayed. It costs no energy to flip one spin in the cluster, $\Delta E=E(\uparrow\uparrow\uparrow\downarrow)-E(\uparrow\downarrow\uparrow\downarrow)=0$, for $t>0$, whereas there is an energy cost of $\Delta E=3|t|$ associated with flipping a spin in the $t<0$ case. We will see in Sec. VI that this tendency to ferromagnetism persists in the noninteracting triangular lattice.

2. *Interacting case* ($U>0$)

For a strongly interacting system the filling factor n will play an important role in the solution. A nontrivial case in the triangle relevant to Na_xCoO_2 is $n=\frac{4}{3}$. The $n=\frac{5}{3}$ case is trivial as is simply the case of a single (and therefore noninteracting) hole, while the half filled case will not be studied in detail in this paper. The relevant basis set is rather different from that for noninteracting particles and we therefore illustrate the solution in Fig. 6 below. To represent this basis set more precisely we will adopt the notation $|\alpha,\beta,\gamma\rangle$ where the values of α, β, and γ indicate the state on the first, second, and third sites, respectively. We allow α, β, and γ to take the values 0, indicating an unoccupied site, $\uparrow$, indicating a site singly occupied with a spin up electron, $\downarrow$, indicating a site singly occupied with a spin down electron, and $\uparrow\downarrow$ which indicates a doubly occupied site.[55] For $t<0$ we find that for any finite U the ground state has energy[56]

$$E_-=\frac{1}{2}(2t+3U-\sqrt{36t^2-4tU+U^2}) \tag{3}$$

and is a superposition of singlets

$$|\Psi_-\rangle=\frac{1}{A}\sin\theta[|\uparrow\downarrow,\uparrow\downarrow,0\rangle+|\uparrow\downarrow,0,\uparrow\downarrow\rangle+|0,\uparrow\downarrow,\uparrow\downarrow\rangle]+\frac{1}{A}\cos\theta[(|\uparrow\downarrow,\uparrow,\downarrow\rangle-|\uparrow\downarrow,\downarrow,\uparrow\rangle)+(|\uparrow,\uparrow\downarrow,\downarrow\rangle-|\downarrow,\uparrow\downarrow,\uparrow\rangle)+(|\uparrow,\downarrow,\uparrow\downarrow\rangle-|\downarrow,\uparrow,\uparrow\downarrow\rangle)], \tag{4}$$

where

$$\tan\theta=\frac{U+6t-\sqrt{36t^2-4tU+U^2}}{U-6t+\sqrt{36t^2-4tU+U^2}}, \tag{5}$$

and the normalization factor is $A=\sqrt{3+3\cos^2\theta}$. Clearly, $\theta\to 0$ as $U\to\infty$ and $\theta\to-\pi/4$ as $U\to 0$. We sketch this wave function in the lower part of Fig. 3.

$|\Psi_-\rangle$ is a superposition of the resonating valence bond state and the states with two doubly occupied sites. The fact that $\theta\to 0$ as $U\to\infty$ indicates that the amplitude for having two doubly occupied sites vanishes in this limit as one expects. Clearly $|\Psi_-\rangle$ has no net magnetization, and this state leads to the paramagnetic state found in the thermodynamic limit for $t<0$ (cf. Fig. 1). $|\Psi_-\rangle$ has significant short-range antiferromagnetic spin fluctuations, which are not captured in the purely local DMFT treatment that follows, although it is likely that these persist in the true thermodynamic ground state (see Sec. II A).

For any finite U and $t>0$ the ground state has energy $E_+=-2t+U$ and is threefold degenerate. All three states are spin 1 and three degenerate states correspond to $S_z=-1$, 0, and 1. The respective eigenstates correspond to superpositions of triplets and are

$$|\Psi_+^{\downarrow}\rangle=\frac{1}{\sqrt{3}}[|\uparrow\downarrow,\downarrow,\downarrow\rangle-|\downarrow,\uparrow\downarrow,\downarrow\rangle+|\downarrow,\downarrow,\uparrow\downarrow\rangle], \tag{6}$$

$$|\Psi_+^{0}\rangle=\frac{1}{\sqrt{6}}[(|\uparrow\downarrow,\uparrow,\downarrow\rangle+|\uparrow\downarrow,\downarrow,\uparrow\rangle)-(|\uparrow,\uparrow\downarrow,\downarrow\rangle+|\downarrow,\uparrow\downarrow,\uparrow\rangle)+(|\uparrow,\downarrow,\uparrow\downarrow\rangle+|\downarrow,\uparrow,\uparrow\downarrow\rangle)], \tag{7}$$

and

$$|\Psi_+^{\uparrow}\rangle=\frac{1}{\sqrt{3}}[|\uparrow\downarrow,\uparrow,\uparrow\rangle-|\uparrow,\uparrow\downarrow,\uparrow\rangle+|\uparrow,\uparrow,\uparrow\downarrow\rangle]. \tag{8}$$

These wave functions are illustrated in the upper part of Fig. 3.

$|\Psi_+^{\downarrow}\rangle$, $|\Psi_+^{0}\rangle$, and $|\Psi_+^{\uparrow}\rangle$ display short range ferromagnetic fluctuations for all finite U, in particular the total spin of the system is a maximum along one axis as the ground state consists of a superposition of triplets. As the ferromagnetism

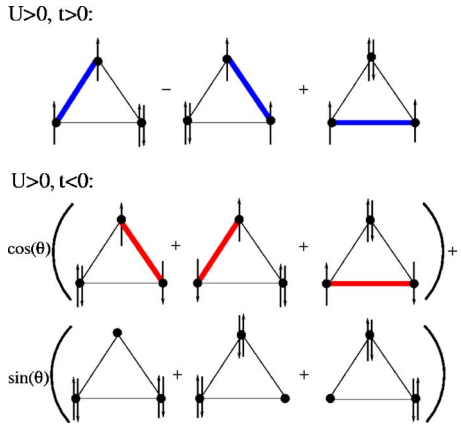

FIG. 3. (Color online) A pictorial representation of the ground states of the Hubbard model on a triangular cluster with four electrons. Doubly occupied sites are indicated by the presence of two arrows, one pointing up and the other pointing down, while unoccupied sites have no arrows. In the cases where we have only one doubly occupied site the remaining sites with only one electron can form either a singlet (indicated by a thick red line with arrows on the two sites pointing in opposite directions) or a triplet (indicated by a thick blue line with arrows on the two sites pointing in the same direction). Thus, the middle left triangle indicates the state $\frac{1}{\sqrt{2}}(|\uparrow\downarrow,\uparrow,\downarrow\rangle-|\uparrow\downarrow,\downarrow,\uparrow\rangle)$. The top left triangle indicates one the three states $|\downarrow,\downarrow,\uparrow\downarrow\rangle$, $\frac{1}{\sqrt{2}}(|\uparrow,\downarrow,\uparrow\downarrow\rangle+|\downarrow,\uparrow,\uparrow\downarrow\rangle)$ or $|\uparrow,\uparrow,\uparrow\downarrow\rangle$ (Ref. 55). To keep the figure as simple as possible we have not included normalization factors in the figure, but the correct normalizations are given in Eqs. (4) and (6)–(8). The lower part of the figure illustrates $|\Psi_-\rangle$, the ground state for any nonzero value of U and $t<0$ [cf. Eq. (4)] (the ground state is degenerate for $t<0$ and $U=0$). The upper part of the figure illustrates all three degenerate states $|\Psi_+^{\downarrow}\rangle$, $|\Psi_+^{0}\rangle$, and $|\Psi_+^{\uparrow}\rangle$ as these only differ by the value of the $S_z=0$ projection of the triplet. These states are the ground states for $t<0$ and any value of U [cf. Eqs. (6)–(8)]. $|\Psi_-\rangle$ depends on the variable θ which is a function of the ratio U/t, given by Eq. (5). $\theta\to 0$ as $U\to\infty$; $\theta=\pi/4$ for $U=0$.

is associated with kinetic energy frustration, we have a Nagaoka-type ferromagnet for any finite value of U. In the calculations for the infinite triangular lattice with $t>0$ presented below we will again see this type of magnetism for some fillings, but with a phase transition from a Curie-Weiss metal to a Nagaoka ferromagnet at some finite value of U, as is shown in Fig. 1.

In order to quantify the nature and magnitude of the spin interactions induced by the correlations we evaluate the expectation value of $\vec{S}_i\cdot\vec{S}_j$ for neigboring sites on the triangle. We find that for $t>0$, this expectation value is $1/12$, whereas for $t<0$ it is $-\cos\theta^2/[3(1+\cos\theta^2)]$ which becomes more negative with increasing U and tends to $-1/6$ for $U\gg|t|$. For reference, for the two site Hubbard model, with two electrons, this expectation value is always negative, regardless of the sign of t, indicating antiferromagnetic spin correlations. Here, we see that for the triangular cluster, the sign of t determines whether the nearest neighbor spin correlations are ferromagnetic or antiferromagnetic.

III. DYNAMICAL MEAN-FIELD THEORY

A. Relevance of DMFT to the two-dimensional triangular lattice

Before presenting our results an important issue to address is the relevance of DMFT to model (1) which describes a two-dimensional system. DMFT is only exact in infinite dimensions or for a lattice with infinite coordination number. We will see below that an important role of the triangular lattice, as compared to other, nonfrustrated, lattices, is not just that the shape of the bare DOS changes (which is extremely important) but also to make DMFT a good approximation.

DMFT has become an important tool in the description of strongly correlated systems. It has provided a realistic description of transport and dynamical properties of materials such as transition metal oxides and layered organic superconductors with frustrated lattices such as κ-(BEDT-TTF)$_2X$, where X is an anion, e.g., I_3 or $Cu_2(CN)_3$. The κ-(BEDT-TTF)$_2X$ family have a phase diagram (as a function of pressure, uniaxial stress, or chemical substitution) in which a superconducting phase is in close proximity to a Mott insulating phase. In the metallic phase of the κ-(BEDT-TTF)$_2X$ there is a temperature scale, T^*, at which there is a smooth crossover from a Fermi liquid to an incoherent "bad metal" [characterized by the absence of a Drude peak in the frequency dependent conductivity, a resistivity of the order of the Ioffe-Regel-Mott limit ($\hbar/e^2a$, where a is the lattice constant), a thermopower of the order of $k_B/|e|$, and a nonmonotonic temperature dependence of the thermopower and resistivity].[22,59] The temperature dependence of transport properties displays a crossover from coherent Fermi liquid behavior to incoherent excitations. In the case of the organic superconductors it has been found that the DMFT of the Hubbard model gives both a qualitative[22] and quantitative[59] description of this crossover from a Fermi liquid to a "bad metal" in which there are no quasiparticles.

The crossover temperature scale is related to the destruction of Kondo screening and Fermi liquid behavior with increasing temperature (above the Kondo temperature T_K) in the Anderson model (which is the effective model solved in the DMFT equations as described above). In the Anderson model the conduction electrons are strongly scattered by a (localized) magnetic impurity for $T>T_K$. But for $T<T_K$ a singlet forms between the impurity and the conduction electrons. In the DMFT of the Hubbard model for $T>T^*$ the electrons are quasilocalized and the electrons on the single site treated exactly strongly scatter those in the bath. However, for $T<T^*$, transport is coherent and the electrons only scatter one another weakly, thus Fermi liquid behavior is regained.

The success of DMFT in describing the transport properties and the phase diagram of many organic charge transfer salts down to temperatures of about 10–20 K (where, for example, superconductivity becomes important) has been rather puzzling given that these materials are quasi-two-dimensional and DMFT is only expected to be a good approximation in the limit of high dimension or coordination number. However, the applicability of DMFT to low-

dimensional systems with large frustration is consistent with the fact that for frustrated magnetic models a Curie-Weiss law holds down to a much lower temperature than for unfrustrated models[60–62] indicating the presence of well formed local moments. Recently, Zheng *et al.*[62] calculated the temperature dependence of the magnetic susceptibility of the antiferromagnetic Heisenberg model on an anisotropic triangular lattice. They found that for models close to the isotropic triangular lattice (i.e., models with significant magnetic frustration) that the Curie-Weiss law (which is a mean-field, single site approximation) holds down to relatively low temperatures. Deviations from Curie-Weiss behavior result from spatially dependent correlations. Hence, we expect that a DMFT treatment of the Hubbard model on the triangular lattice will be a good approximation down to much lower temperatures than unfrustrated models. Furthermore, in the "bad metal" region magnetic properties such as the uniform susceptibility and spin relaxation rate, can be described by the Heisenberg model because the electrons are essentially localized due to the proximity to the Mott insulating phase. This means that the susceptibility can be fit to a Curie-Weiss form down to temperatures much less than the exchange energy J. Furthermore, the spin correlation length of the antiferromagnetic Heisenberg model increases with temperature T much more slowly for the triangular lattice than the square lattice.[63] Specifically, at $T=0.3J$ the spin correlation length is only one lattice constant for the triangular lattice. In contrast, for the square lattice the correlation length is about 50 lattice constants, at $T=0.3J$.[63]

The above arguments have been recently tested by means of cluster DMFT calculations. These calculations show how for the isotropic triangular lattice the solution coincides with single site DMFT (in particular a quasiparticle peak appears at the Fermi energy). However, as soon as frustration is released a pseudogap opens up in the one-electron spectra as a result of short range antiferromagnetic correlations.[64]

A further hint that DMFT is a better approximation on the triangular lattice than on the square lattice comes from the fact that we find that at half filling our calculations predict that the Mott transition occurs at $U_c \approx 15|t|$ (see Figs. 1 and 9). This compares with exact diagonalization studies on 12 site lattices[32] which find that the Mott transition takes place at $U \approx 12|t|$. On the square lattice it is known that perfect nesting means that the ground state is a Mott insulator for any finite U. However, DMFT predicts[20] that $U_c \approx 12|t|$ unless antiferromagnetism is included. Thus (without including antiferromagnetism) DMFT gives a qualitatively incorrect result for the (unfrustrated) square lattice, but a qualitatively correct result for the (frustrated) triangular lattice.

B. Formalism

The electronic and magnetic properties of the Hubbard model on the triangular lattice (1) are analyzed below using DMFT.[20] Previously, various properties of doped Mott insulators on an hypercubic lattice have been explored within DMFT in the context of the high-T_c superconductors[21] using Quantum Monte Carlo (QMC) techniques. Here, we apply DMFT to a frustrated lattice and use exact diagonalization and Lanczos techniques to solve the associated Anderson impurity problem[57] at finite and zero temperature, respectively.

We will now briefly describe the DMFT formalism focusing on the relevant equations and quantities of interest in this work. For a more detailed discussion see, for example, Ref. 20. DMFT treats the quantum dynamics on a single site exactly and the remaining lattice sites provide a bath with which this site interacts. One may map the Hubbard model onto an Anderson single-impurity model which must be solved self-consistently. The bath is described through the Weiss field, $G_{0\sigma}(i\omega_n)$. The iterative procedure starts by solving the Anderson model for a given choice of $G_{0\sigma}(i\omega_n)$. From the on-site Greens function, $G_\sigma(i\omega_n)$ we may obtain the self-energy of the system

$$\Sigma_\sigma(i\omega_n) = G_{0\sigma}^{-1}(i\omega_n) - G_\sigma^{-1}(i\omega_n), \tag{9}$$

which is used to describe the lattice propagator

$$G_\sigma(i\omega_n) = \sum_{\mathbf{k}} G_\sigma(\mathbf{k}, i\omega_n) \tag{10}$$

$$= \sum_{\mathbf{k}} \frac{1}{i\omega_n + \mu - \epsilon_{\mathbf{k}} - \Sigma_\sigma(i\omega_n)}, \tag{11}$$

where μ is the chemical potential, $\omega_n = (2n+1)\pi/\beta$ is a Matsubara fermionic frequency, and $\beta = 1/k_B T$. The above procedure is repeated until a self-consistent solution for the lattice propagator is found.

1. Magnetic susceptibilities

The magnetization of the system under a small magnetic field, h, is computed from

$$m = \mu_B (n_\uparrow - n_\downarrow), \tag{12}$$

where $n_\uparrow$ and $n_\downarrow$ are obtained from the DMFT solution at self-consistency.

The uniform ($\mathbf{q}=0$) susceptibility is then obtained numerically[58] from

$$\chi(T) = \lim_{h\to 0} \frac{\partial m}{\partial h}. \tag{13}$$

It is interesting to compare the uniform susceptibility with the local susceptibility obtained from

$$\chi_{\mathrm{loc}}(T) = \sum_{\mathbf{q}} \chi(\mathbf{q}) = \mu_B^2 \int_0^\beta \langle S_z(0) S_z(\tau)\rangle d\tau, \tag{14}$$

where $S_z(\tau) = n_\uparrow(\tau) - n_\downarrow(\tau)$.

The local susceptibility in the imaginary frequency axis is given by

$$\chi_{\mathrm{loc}}(i\omega_n) = \mu_B^2 \int_0^\beta e^{-i\omega_n \tau} \langle S_z(0) S_z(\tau)\rangle d\tau. \tag{15}$$

The frequency-dependent local magnetic susceptibility is related[20] to the nuclear magnetic resonance (NMR) Knight shift $K(T)$ by

$$K(T) = A \lim_{\omega \to 0} \mathrm{Re}\, \chi_{\mathrm{loc}}(\omega + i\eta) \tag{16}$$

when the hyperfine interaction A form factor is independent of the wave vector, i.e., in the local limit appropriate to DMFT. The NMR relaxation rate $1/T_1$ is given by

$$\frac{1}{T_1 T} \propto \lim_{\omega \to 0} \frac{1}{\pi} \frac{\mathrm{Im}\, \chi_{\mathrm{loc}}(\omega + i\eta)}{\omega}, \tag{17}$$

where ω is a real frequency and η is an arbitrarily small real number.

2. Numerical methods

Due to the rapid convergence of the solution with the bath size[57] it is sufficient to use a discrete set of states of $n_s = 6-10$ sites to model the electronic bath in order to obtain reliable results. In what follows we use Lanczos diagonalization on $n_s = 8$ sites to calculate zero temperature properties. In Sec. IV we also present results for high temperatures for which the Lanczos technique is not adequate, we therefore use exact diagonalization to solve the Anderson impurity problem. However, as exact diagonalization is more computationally expensive than Lanczos diagonalization we are limited to $n_s = 6$ for these calculations. Further it is well known[20] that for exact diagonalization there is a low energy scale $T^{ns} = E_1 - E_0$, where E_0 and E_1 are respectively the ground state energy and the energy of the first excited state of the system (recall that there is a finite energy gap to the first excited state because of the finite bath size), below which the results of exact diagonalization calculations are not trustworthy. We therefore present exact diagonalization results for finite temperatures with $T > T^{ns}$ and Lanczos data valid in the $T \to 0$ limit. Combining the two methods allows us to have a rather complete description of the T-dependence of various properties.

IV. TEMPERATURE DEPENDENCE OF MAGNETIC SUSCEPTIBILITY

We now analyze the behavior of the uniform and local magnetic susceptibilities obtained from DMFT for the Hubbard model on the triangular lattice for both $t > 0$ and $t < 0$. We find that the two different signs of the hopping integral lead to very different magnetic responses (cf. Fig. 1) and that Curie-Weiss metallic behavior appears when $t > 0$ but not for $t < 0$.

A. Local magnetic susceptibility

The degree of localization of the electrons in the triangular lattice with different signs of t can be explored by computing the imaginary time, τ, local spin autocorrelation function,

$$H(\tau) \equiv \langle S_z(0) S_z(\tau) \rangle. \tag{18}$$

Such a correlation function can be related to a spectral density $A(\omega)$ by[65]

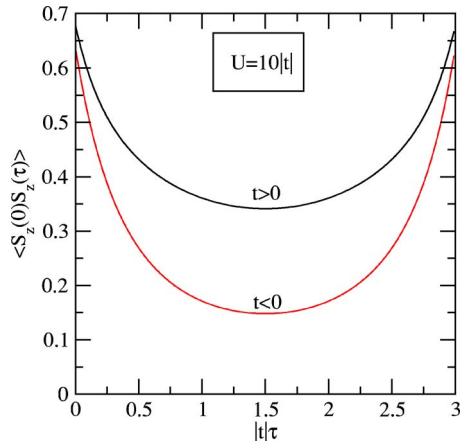

FIG. 4. (Color online) The imaginary time local spin autocorrelation function for both $t > 0$ and $t < 0$ with $n = 1.3$, $U = 10|t|$ and $\beta = 3/|t|$. The larger values of $\langle S_z(0) S_z(\tau = \beta/2) \rangle$ for $t > 0$ than for $t < 0$ indicates the greater degree of localization of the electrons for $t > 0$.

$$H(\tau) = \frac{1}{2\pi} \int_{-\infty}^{\infty} d\omega \exp(-\omega\tau) \frac{A(\omega)}{1 - e^{-\beta\omega}}. \tag{19}$$

If $A(\omega) = -A(-\omega)$, then

$$H(\tau) = \frac{1}{2\pi} \int_{0}^{\infty} d\omega \frac{A(\omega)[e^{-\omega\tau} + e^{-(\beta-\tau)\omega}]}{1 - e^{-\beta\omega}}. \tag{20}$$

It then follows that $H(\tau) = H(\beta - \tau)$, as one expects for the correlation function of commuting operators,[66] and $H(\tau)$ should be symmetric about $\tau = \beta/2$. The function $H(\tau)$ is related to the local susceptibility at Matsubara frequencies by Eq. (15).

The simplest possible form that the frequency dependent local susceptibility $\chi_{\mathrm{loc}}(\omega)$ [compare Eqs. (16) and (17)] can take is a "Drude" type form with a single relaxation rate, Γ, $\chi_{\mathrm{loc}}(\omega) = \chi_0/(1 + i\omega/\Gamma)$, leading to a Lorentzian form for the spectral density. We note that for a single impurity Anderson model it was found that this Drude form of the relaxation rate is a good approximation for temperatures larger than the Kondo temperature.[67]

In a Fermi liquid, $H(\tau) \sim 1/\tau^2$ for $1/\tau \sim 1/\beta \ll T^*$. In a Mott insulator, $H(\tau)$ decays exponentially to a nonzero value for long imaginary times $\tau \sim \beta/2$.[20] The "bad metal" regime represents intermediate behavior, and the value $H(\tau = \beta/2)$ is a measure of the extent to which the electrons are localized.

In the limit in which $\langle S_z(0) S_z(\tau) \rangle$ becomes constant one obtains from Eq. (14),

$$\chi_{\mathrm{loc}}(T) = \frac{\mu_B^2}{T}, \tag{21}$$

recovering the Curie law for localized magnetic moments. In Fig. 4 we have plotted $\langle S_z(0) S_z(\tau) \rangle$ for $U = 10|t|$, $n = 1.3$ at inverse temperature of $\beta = 3/|t|$, for both $t > 0$ and $t < 0$. Indeed we find that electrons for the $t > 0$ triangular lattice (weak τ dependence) are more localized than those in the t

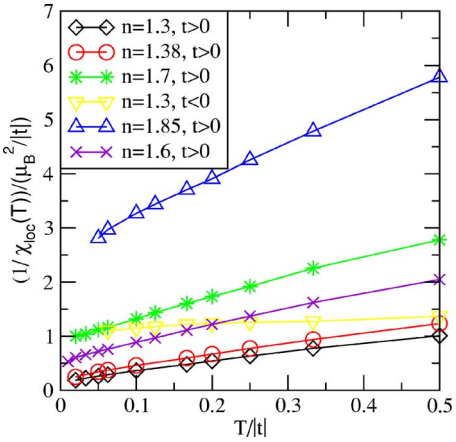

FIG. 5. (Color online) The temperature dependence of the inverse of the local spin susceptibility for different electron occupations, n. We present results for $U=10|t|$ and for both $t<0$ and $t>0$. The lines are guides to the eye. For the $t>0$ cases (only $n=1.3$ is shown for clarity) the coherence temperature $T^* \ll |t|$, whereas for the $t<0$ cases $T^* \sim |t|$.

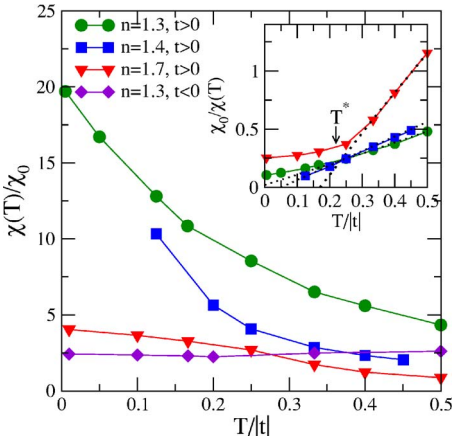

FIG. 6. (Color online) Curie-Weiss versus paramagnetic behavior of the uniform susceptibility, $\chi(T)$, for the Hubbard model on the triangular lattice with $U=10|t|$. The inset shows $\chi_0/\chi(T)$ (where χ_0 is the zero temperature noninteracting magnetic susceptibility). The central panel compares the strong T dependence for $t>0$ with the nearly temperature independent behavior for $t<0$ (Pauli paramagnetism). For $n=1.4$ ferromagnetism appears below a critical temperature, T_c. The main panel displays the inverse of the uniform susceptibility, $\chi_0/\chi(T)$, showing the Curie-Weiss T dependence for $t>0$. The arrow indicates the coherence temperature T^* found from fitting the local susceptibility data in Fig. 5 to Eq. (22).

<0 case (strong τ dependence). Both curves are symmetric about $\tau=\beta/2$ as is required.

We find that $\langle S_z(0)S_z(\tau)\rangle$ is not constant for either sign of t which reflects spin relaxation processes and the fact that electrons are not completely localized. The actual behavior at large temperatures is not the pure Curie behavior of Eq. (21) but rather, to a good approximation, can be fitted to the Curie-Weiss form

$$\chi_{\rm loc}(T) \sim \frac{\mu_{\rm loc}^2}{T+T^*(n)}, \tag{22}$$

where $T^*(n)$ is again the coherence scale.

In Fig. 5 we plot $1/\chi_{\rm loc}(T)$ from the actual numerical results obtained from DMFT for different electron occupation comparing $t>0$ with the $t<0$ case. Over a broad temperature range the temperature dependence is consistent with a Curie-Weiss form. However, the coherence scale is much larger for $t<0$ than for $t>0$.

B. Uniform magnetic susceptibility

In Fig. 6 we show the temperature dependence of $\chi(T)/\chi_0$ for the triangular lattice with $t>0$ and $U=10|t|$, where χ_0 is the noninteracting uniform susceptibility of the triangular lattice. We find that the temperature dependence of the uniform magnetic susceptibilities are very different for the different signs of the hopping integral. The magnetic susceptibility displays Curie-Weiss behavior at large temperatures when $t>0$, whereas for $t<0$, $\chi(T)$ displays the Pauli paramagnetism characteristic of a weakly correlated metal.

We now discuss the $t>0$ case in more detail. To be specific, for $t>0$ and at high temperatures, the uniform susceptibility can be fitted to the expression

$$\chi(T) \simeq \frac{\mu^2}{T+\theta(n)}, \tag{23}$$

where $\theta(n)$ and μ depend on U and n. Note that the temperature scale $\theta(n)$ reduces to $\theta(n)=-T_C$, where T_C is the critical temperature at which the ferromagnetic transition occurs for certain values of n, ($1.35 \lesssim n \lesssim 1.6$ for $U=10|t|$; see Sec. VI for details). The Curie-Weiss behavior described by Eq. (23) is valid for large temperatures, $T>T^*(n)$. This is because in this temperature regime the electronic system behaves like a set of quasilocalized magnetic moments. For $T<T^*(n)$ the Curie-Weiss behavior crosses over to a behavior more reminiscent of a renormalized Fermi liquid with a weak temperature dependence. Fitting our results to Eq. (23) for $T>T^*(n)$, gives $\theta(n=1.7)\approx -0.17|t|$ and $\theta(n=1.3)\approx 0.01|t|$ for $n=1.3$. For the ferromagnetic metal appearing for, say, $n=1.38$, the transition to a ferromagnetic metal occurs at $T_C=-\theta(n=1.4)\approx 0.05|t|$. The effective magnetic moment, μ obtained from the fitting varies between $\mu=0.7\mu_B$ for $n=1.3$ and $\mu=0.4\mu_B$ for $n=1.7$.

As n is increased one expects that the average moment will be roughly proportional to the density of unpaired electrons, $2-n$, at each lattice site. Thus μ^2 is suppressed with increasing n and fixed U. Hence one expects that μ^2 varies between $\mu=\mu_B$ for $n=1$ (half-filled system) and $\mu=0$ for $n=2$ (filled band). This is consistent with the values of μ obtained from the fit of Eq. (23) to our numerical results (see the inset of Fig. 7). As the temperature is decreased the susceptibility changes its behavior so that $\chi_0/\chi(T)$ becomes less dependent on temperature (this is most obvious for $n=1.7$). A crossover from Curie-Weiss behavior at high temperatures to Fermi liquid behavior at low temperatures is encountered.

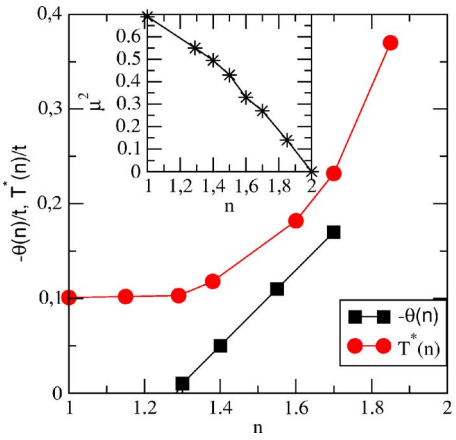

FIG. 7. (Color online) Electron occupation dependence of the coherence scale, $T^*(n)$, the Curie-Weiss scale $\theta(n)$ and the effective moment in the uniform magnetic susceptibility, μ for fixed $U=10|t|$ and $t>0$. These parameters are extracted by fitting the results of our DMFT calculations of magnetic susceptibilities to Eqs. (22) and (23). For these values of U and t ferromagnetism is observed in the range $1.3<n<1.6$ (cf. Fig. 1). $\theta(n)>0$ for $n<1.3$ and no ferromagnetism is found at these dopings. μ decreases to zero as $n\to 2$ as the density of unpaired electrons decreases. This appears to be responsible for the absence of ferromagnetism for $n>1.6$.

The properties of the Fermi liquid state (e.g., effective mass renormalization, susceptibility enhancement) at low temperature will be discussed in the following section.

In Fig. 7 we show a plot of both temperature scales obtained from fitting our data to the Curie-Weiss laws of Eqs. (22) and (23) to obtain, $T^*(n)$ and $\theta(n)$, respectively. $T^*(n)$ increases with the electron occupancy. This is to be expected as the system becomes more weakly correlated in the $n\to 2$ limit, remaining coherent at temperatures comparable with the noninteracting Fermi temperature. On the other hand, $\theta(n)$ can change sign, which is related to the effective short range magnetic coupling, $J(n)$, present in the uniform susceptibility, $\chi(T)$, that does not appear in $\chi_{\rm loc}(T)$. This can be better understood by splitting $\theta(n)$ into[20]

$$\theta(n) \sim T^*(n) + J(n). \tag{24}$$

As the system is driven closer to the Mott insulating state: $n\to 1$, $\theta(n)\to J(n)$ as $T^*(n)\to 0$ which indicates the metal-insulator transition. In this limit the system behaves as a Heisenberg antiferromagnet with antiferromagnetic exchange coupling given by $J=4t^2/U$, with $U>|t|$. A change of sign in $\theta(n)$ happens at about $n=1.3$ in Fig. 7 signaling a ferromagnetic exchange interaction. Indeed, this is approximately the doping at which the ferromagnetic state is found for $U=10|t|$ (cf. Fig. 1). Thus, as the electronic occupation increases, $\theta(n)$ changes from positive (antiferromagnetic) to negative (ferromagnetic) when $J<-T^*$. This is the threshold ferromagnetic interaction for the "bad metal" to become ferromagnetic. At larger doping values the absolute yields of the magnetic moment, μ, become suppressed as the number of unpaired electrons is reduced becoming $\mu\to 0$ as $n\to 2$ which coincides with the destruction of ferromagnetism.

In contrast to the rather unconventional metallic state found for $t>0$, the magnetic susceptibility for $t<0$ is Pauli-like, moderately enhanced by many-body effects. This can be observed in the inset of Fig. 6 where a weak temperature dependence for all n (for clarity only $n=1.3$ is shown) is found. To be specific, for $T\ll\epsilon_F$ the low temperature behavior of the susceptibility for a noninteracting metal is given by[68]

$$\frac{\chi(T)}{\chi_0} \approx 1 + \left(\frac{\rho''(\epsilon_F)}{\rho(\epsilon_F)} - \frac{\rho'(\epsilon_F)^2}{\rho(\epsilon_F)^2}\right)\frac{\pi^2}{6}k_B^2T^2 + O(T^4), \tag{25}$$

where $\rho(\epsilon)$ is the density of states per spin and the primes indicate derivatives of the DOS with respect to ϵ. The noninteracting susceptibility at zero temperature is given by $\chi_0=2\mu_B^2\rho(\epsilon_F)$. For $t<0$ a direct evaluation of the term proportional to T^2 gives nearly zero for electron doping the triangular lattice. Our numerical results agree with temperature dependence given by Eq. (25), with a moderate enhancement of $\chi(T)/\chi_0$ suggesting moderate many-body effects. Hence, we conclude that the $t<0$ electron doped triangular lattice behaves as a renormalized paramagnetic metal.

V. RENORMALIZATION OF QUASIPARTICLES FOR DIFFERENT SIGNS OF t

DMFT typically predicts a metal-insulator transition as U is increased to $U/W\sim 1$ at half-filling.[20] As soon as the system is doped away from half-filling, the system becomes metallic[21] with electrons having their mass renormalized by the Coulomb interaction. We find that the two different densities of states corresponding to the two different signs of t lead to different renormalizations of the quasiparticles although $W=9|t|$ is the same for both DOS. This result is in contrast to the half-filled and unfrustrated cases where the results do not depend on the sign of t. This is because for unfrustrated lattices particle-hole symmetry is respected, whereas particle-hole symmetry is broken on the doped triangular lattice. Half-filled frustrated lattices are *not* particle-hole symmetric, but this asymmetry is suppressed at large U, and particularly in the Mott insulating state.

In order to understand the electronic properties and different magnetic behavior obtained for $t<0$ and $t>0$ (above), the imaginary part of the self-energy along the imaginary axis, $\mathrm{Im}\,\Sigma(i\omega)$ for $t<0$ and $t>0$ is computed and shown in Fig. 8 for $U=10|t|$. The quasiparticle weight can be extracted from the slope of the self-energy,

$$Z = \lim_{\omega\to 0}\left[1 - \frac{\partial\,\mathrm{Im}\,\Sigma(i\omega)}{\partial(i\omega)}\right]^{-1}. \tag{26}$$

The increasing slope at low frequencies of $\mathrm{Im}\,\Sigma(i\omega)$ as $n\to 1$ indicates a stronger renormalization of the quasiparticles as the system gets closer to the Mott metal-insulator transition. This behavior is apparent for both signs of t. However, for $t>0$ electrons are more strongly renormalized than for $t<0$. For example, for $n=1.3$ the slope of $\mathrm{Im}\,\Sigma(i\omega)$ as $\omega\to 0$ is steeper by a factor of about 2 for $t>0$ than it is for $t<0$.

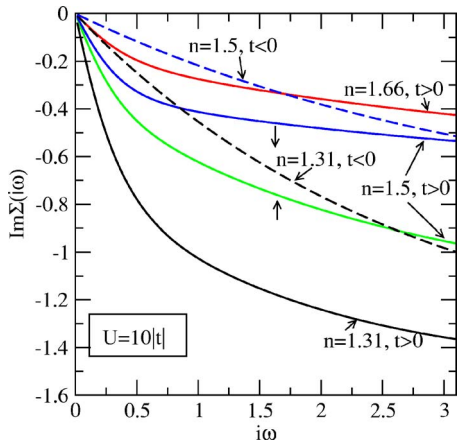

FIG. 8. (Color online) Comparison of the imaginary part of the self-energy for $t>0$ with the same quantities with $t<0$. Results are reported for $U=10|t|$ and various electron dopings. The linear dependence of the self-energy at low energies indicates Fermi liquid behavior. The slope near $i\omega=0$ is used to extract the quasiparticle weight Z, shown in Fig. 9.

A. Effective mass

The quasiparticle weight extracted from the self-energy as a function of the Coulomb interaction U is shown in Fig. 9. Z is compared for $t>0$ and $t<0$ when $n=1.3$. The effective mass is defined by $m^*=m_b/Z$; where m_b is the noninteracting band mass. For $U=10|t|$ we find for $t<0$, $m^*=1.5m_b$, whereas for $t>0$, $m^*=3.4m_b$. For $n=1$ we find $m^*=4.0m_b$ independent of the sign of t. This is an important point as it shows that for the same U/W the two different signs of t lead to different renormalizations of the electrons. Within DMFT this different renormalization of the quasiparticles can be understood from the fact that for electron doping the DOS close

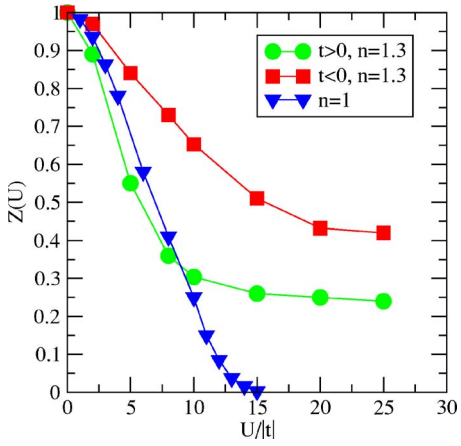

FIG. 9. (Color online) Dependence of the quasiparticle weight Z on the Coulomb repulsion $U/|t|$ at various electron dopings. The quasiparticles become more renormalized as the doping is decreased due to the proximity to the Mott transition. For a given value of U, quasiparticles on the triangular lattice with $t<0$ are less renormalized than for $t>0$. In contrast, for the half-filled case ($n=1$), we find the same behavior of Z for both $t>0$ and $t<0$ with a Mott metal-insulator transition taking place at a common value $U/W\sim 1.66$.

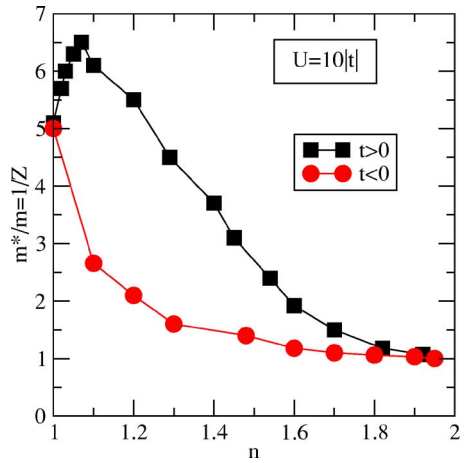

FIG. 10. (Color online) The variation of the effective mass, $m^*/m_b=1/Z$ with doping n for both signs of t for $U=10|t|$. Notice in particular the nonmonotonic variation of the effective mass with n for $t>0$.

to the Fermi energy is larger for $t>0$ than for $t<0$ (cf. the bare DOS shown in Fig. 6).

The different renormalization of the electrons found for the different signs of t in the electron doped system is in contrast to the very similar renormalization found in the half-filled case ($n=1$) for which Z decreases rapidly and in the same way for both $t>0$ and $t<0$, leading to a very similar critical value of $U_c\approx 1.65W$ at which the Mott transition occurs. This value is similar to DMFT estimates obtained for the Bethe lattice,[20] $U_c\approx(1.5-1.7)W$. The value obtained $U_c=15|t|$ should be compared with the $U_c\approx 12|t|$ obtained from exact diagonalization calculations for 12 site clusters.[32] The similar critical values appearing at half filling can be explained from the fact that as $U\to W$, the spectral densities at each site are strongly modified by the Coulomb interaction washing out the fine details of the bare DOS. In contrast, for the doped case, kinetic energy effects are important.

In Fig. 10 we show the variation of the effective mass with n for $U=10|t|$. Strikingly the effective mass *increases* when the system is doped off half-filling close to $n=1$ and $t>0$ displaying a maximum at about $n=1.07$. This is in contrast to the $t<0$ case, and what has been found previously for nonfrustrated lattices such as the hypercubic lattice, for which the effective mass decreases as the system is doped away from half-filling, reflecting reduced correlations. In fact, for $n>1.07$ and $t>0$ the effective masses do decrease with increasing n, reaching the noninteracting limit ($Z\to 1$), as $n\to 2$. A nonmonotonic behavior of the effective mass is then found close to half-filling and $t>0$. This is in contrast to the simple behavior encountered for the hole doped ($n<1$) Mott insulator with a flat noninteracting DOS. In that case, the effective mass behaves as[20]

$$m^*/m_b \propto 1/x, \tag{27}$$

diverging at the Mott transition. This result can also be derived from slave-boson theory.[69]

The effective mass increase with initial doping is a result of the initial increase of the DOS for $t>0$ as ϵ_F moves closer

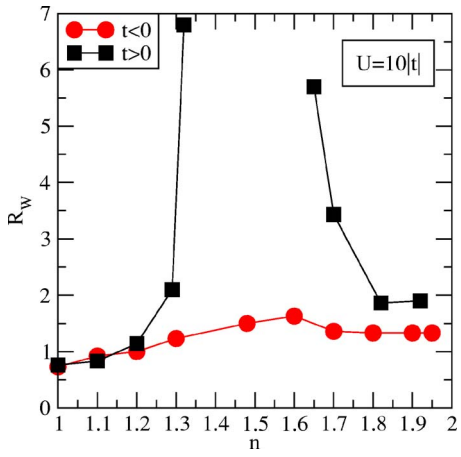

FIG. 11. (Color online) The variation of the Sommerfeld-Wilson ratio, $R_W = \lim_{T\to 0}(\chi(T)/\chi_0)/(\gamma(T)/\gamma_0)$ with doping n for both signs of t for $U=10|t|$.

to the van Hove singularity. The subsequent decrease in the effective mass can be attributed to the decrease in the effective number of charge carriers which suppresses correlation effects. It would be interesting to see whether slave boson theory, with the DOS for the triangular lattice, could reproduce the nonmonotonic dependence of the quasiparticle weight on doping. [This would involve solving Eqs. (8) and (9) in Ref. 69.]

B. Sommerfeld-Wilson ratio

In order to explore the effect of magnetic exchange in the metallic correlated state we analyze the Sommerfeld-Wilson ratio,

$$R_W = \lim_{T\to 0} \frac{\chi(T)/\chi_0}{\gamma(T)/\gamma_0} = \frac{1}{1+F_0^a}, \tag{28}$$

where F_0^a is the Fermi liquid parameter which is a measure the proximity of the system to a ferromagnetic instability ($F_0^a=-1$ at the instability) and $\gamma/\gamma_0 = 1/Z$. The dependence of R_W on the electron occupation factors are plotted in Fig. 11 for both $t>0$ and $t<0$. The ratio R_W is the same at $n=1$ for $t>0$ and $t<0$ but they behave very differently as the occupation is increased. For the $t>0$ triangular lattice R_W is strongly enhanced signaling the proximity to a magnetic instability at about $n=1.35$ and $n=1.65$ (see the phase diagram in Fig. 1 for $t>0$). For $t<0$, R_W displays a maximum close to $n=1.5$.

C. Spectral density

The different renormalization of the electrons for different signs of t is translated onto a different redistribution of spectral weight induced by the Coulomb interaction as the spectral weight suppressed at the Fermi energy must be transferred to higher energies. We investigate this by computing local spectral densities, $A_\sigma(\omega) = -\frac{1}{\pi}\,\mathrm{Im}\,G_\sigma(\omega + i\eta)$, where η is an arbitrarily small real number and

$$G_\sigma(i\omega) = \int_{-\infty}^{\infty} \frac{d\epsilon \rho(\epsilon)}{i\omega + \mu - \epsilon - \Sigma_\sigma(i\omega)}. \tag{29}$$

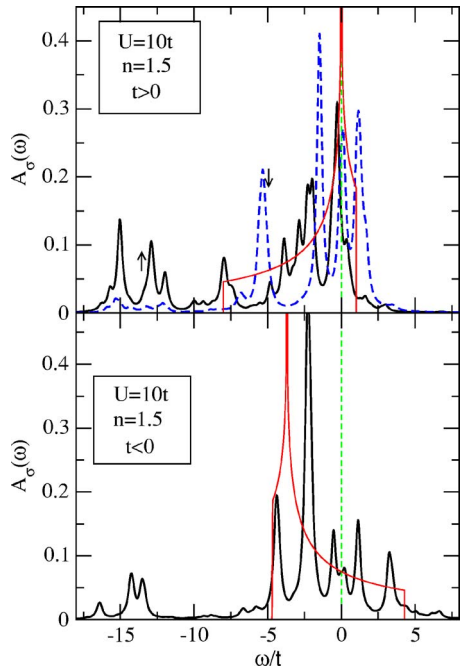

FIG. 12. (Color online) Spectral densities for $U=10|t|$ and $n=1.5$ for the triangular lattice with $t<0$ and $t>0$. The noninteracting DOS is also shown (red line) for comparison and energies are relative to the Fermi energy. The majority (↑) and minority (↓) spectral densities for $n=1.5$ and $t>0$ are shown as the system is ferromagnetic.

In Fig. 12 a comparison of the spectral density $A_\sigma(\omega)$ with the noninteracting DOS per spin, $\rho(\epsilon)$, is made for the case $n=1.5$ and $U=10|t|$. For these parameters ferromagnetism occurs when $t>0$. Notice that within the ferromagnetic metallic phase the spectral function of majority spin subband (↑) is found to be renormalized more strongly than that of the minority spin subband (↓). The lower Hubbard band for spin up electrons contains more spectral weight than the lower Hubbard band for spin down electrons. One may view this effect as originating from the preclusion of the hopping of a minority spin hole to a neighboring site by the presence of a minority spin hole.

D. Resistivity and Kadowaki-Woods ratio

Within the DMFT approximation the conductivity is given by[20]

$$\sigma(T) = \frac{e^2\pi}{\hbar V}\int_{-\infty}^{\infty} d\omega \left(\frac{-\partial f(\omega)}{\partial \omega}\right) \sum_{\mathbf{k}\sigma} \left(\frac{\partial \epsilon_{\mathbf{k}}}{\partial k_x}\right)^2 A_\sigma(\mathbf{k},\omega)^2, \tag{30}$$

where V is the volume. In the limit of low temperatures, $T\to 0$, the resistivity becomes $\rho \approx AT^2$, with the A coefficient given by

$$A = \frac{\hbar}{e^2}\frac{|C_\Sigma|}{\Phi(\tilde{\epsilon}_F) I}. \tag{31}$$

The dimensionless constant

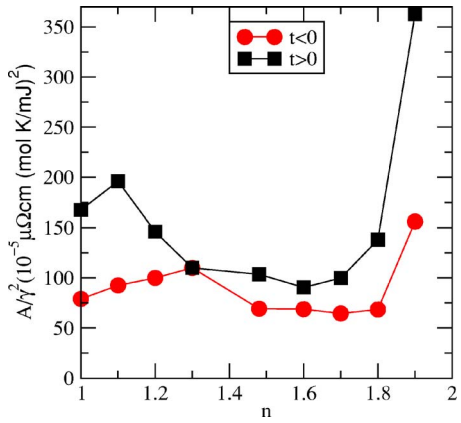

FIG. 13. (Color online) The doping dependence of the Kadowaki-Woods ratio A/γ^2 for $t<0$ and $t>0$ for fixed $U=10|t|$. The lattice parameter, $a=2.84$ Å relevant to Na_xCoO_2 has been used. Note the nonmonotonic doping dependence of the ratio and the fact that even at half-filling the ratios are different for the different signs of t.

$$I=\int_{-\infty}^{\infty}\frac{e^x}{(x^2+\pi^2)(1+e^x)^2}\approx\frac{1}{12},$$

C_Σ is the ω^2 coefficient of the imaginary part of the self-energy, $\mathrm{Im}\,\Sigma(\omega)\approx-|C_\Sigma|(\omega^2+(\pi T)^2)$, and $\Phi(\tilde{\epsilon}_F)$ is given by

$$\Phi(\tilde{\epsilon_F})=\frac{1}{V}\sum_{\mathbf{k}}\left(\frac{\partial\epsilon_{\mathbf{k}}}{\partial k_x}\right)^2\delta(\tilde{\epsilon_F}-\epsilon_{\mathbf{k}}). \tag{32}$$

In the above equations $\tilde{\epsilon}_F=\mu-\mathrm{Re}\,\Sigma(0)=\epsilon_F$, where ϵ_F is the Fermi energy of the noninteracting system[70] for a given electron occupation n. From the T^2 coefficient of the resistivity, A, and the specific heat slope at low temperatures, $\gamma=2\pi^2k_B^2\tilde{A}(\tilde{\epsilon}_F)/3=\pi^2k_B^2\rho(\epsilon_F)/Z$, where $\tilde{A}(\tilde{\epsilon}_F)$ and $\rho(\epsilon_F)$ are the interacting and noninteracting quasiparticle density of states per spin. We can now obtain the Kadowaki-Woods ratio,

$$\frac{A}{\gamma^2}=\frac{\hbar}{e^2}\frac{9|C_\Sigma|Z^2}{4\Phi(\epsilon_F)\pi^4k_B^2I\rho(\epsilon_F)^2}. \tag{33}$$

The doping dependence of the Kadowaki-Woods ratio is plotted in Fig. 13 comparing the $t>0$ and $t<0$ cases. The figure displays the nonmonotonic dependence of the ratio with electron occupation and also how different band structures can lead to different absolute values of the Kadowaki-Woods ratio.

VI. FERROMAGNETISM

Nagaoka rigorously proved[17] that the Hubbard model on a connected lattice[71] in the $U\to\infty$ limit displays ferromagnetism when one hole (electron) is added to the half-filled system when $t<0$ ($t>0$). This is due to the fact that in this case, the kinetic energy is minimized if all the spins are aligned in the same direction. This rigorous treatment has not been extended to doping by more than one hole and it remains an outstanding problem to further understand this interesting phenomenon.[72]

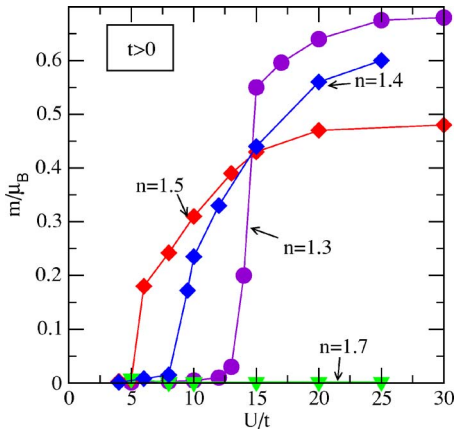

FIG. 14. (Color online) Ferromagnetism in the electron doped $t>0$ triangular lattice from DMFT. The magnitude of the spontaneous magnetic moment is shown as a function of the electron occupation n. As U is increased above $U_c(n)$ the system magnetizes spontaneously stabilizing a ferromagnetic metal in a broad doping region. Ferromagnetism does not appear in the electron doped $t<0$ triangular lattice.

DMFT has proved to be an important tool to describe ferromagnetism appearing due to local electronic correlations. The possibility of Nagaoka or metallic ferromagnetism in a hole doped infinite dimensional fcc lattice has been previously analyzed within DMFT.[73] More recently DFT(LDA)+DMFT calculations (where DFT is density functional theory and LDA is the local density approximation) have provided a realistic description of ferromagnetism in Fe and Ni.[74] Our calculations show that for sufficiently large U and $t>0$ ferromagnetism occurs while the system is still metallic as the spectral density at the Fermi energy is always finite for nonzero doping (cf. Fig. 12). In Fig. 14 we show the sharp ferromagnetic transition in the $T\to0$ limit for $t>0$ obtained from our DMFT calculations.

Increasing U stabilizes the ferromagnetic region in a broader electron occupation range. Ferromagnetism is found to be more stable for $1<n<1.5$ than for $1.5<n<2$, indicating the importance of correlation effects as the system is closer to the Mott insulating phase as $n\to1$ and sufficiently large U. The ferromagnetic transition is found to be sharp as shown in Fig. 14 even at the lowest U value for $n=1.5$ where the van Hove singularity occurs in the bare DOS. In contrast for $t<0$ where, for electron doping, there is no van Hove singularity we do not observe ferromagnetism. This is, of course, rather reminiscent of a Stoner-type instability.

In order to explore the possibility of having Stoner ferromagnetism we can obtain the critical value U_c^S for ferromagnetism from the Hartree-Fock (random phase approximation, RPA) Stoner condition

$$U_c^S(n)\rho(\epsilon_F)=1, \tag{34}$$

where $\rho(\epsilon_F)$ is the bare DOS per spin. One would find $U_c^S(n=1.5)=0$ and $U_c^S(n=1)=5$ for $t>0$ which are much smaller values than the ones obtained from DMFT calculations (see Fig. 1). Furthermore, from the Stoner condition we would also expect a ferromagnetic instability at $U_c^S(n=1.3)$

$=5.26$ and $U_c^S(n=1.90)=10$ for $t<0$. Clearly, simple Stoner ferromagnetism is inconsistent with our DMFT results not only at the quantitative but also qualitative level as the Stoner criterion would predict ferromagnetism for both signs of t for sufficiently large, but finite, values of U. Stoner theory is known to overestimate ferromagnetic tendencies.[75,76] In the present case, it would predict ferromagnetism for $t<0$ in contrast to the more sophisticated DMFT treatment. This difference can be attributed to the on-site dynamical correlation effects which strongly redistribute the spectral weight of the electrons and that are not taken into account in standard mean-field theories.

Vollhardt *et al.*[76] have given a nice review of the essential features of Hubbard models that are favorable towards to ferromagnetism. (i) The energy dependence of the density of states near the Fermi energy should be sufficiently asymmetric, with the DOS being larger towards the top (bottom) of the band for electron (hole) doping. A flat band system with a singular DOS at the upper (lower) edge the most favorable for ferromagnetism. Then the increase in electronic kinetic energy associated with spin polarization is smaller than for a constant DOS. (ii) Strong Coulomb interactions narrow the bands. Less narrowing occurs for the polarized case because polarization reduces the effect of correlations.

Our DOS is not of the flat band type, however, the energy cost in completely polarizing the noninteracting electron doped system for $t>0$ is found to be much smaller than for $t<0$. Indeed, for an electron doped system this is given by

$$\Delta E = 2\int_{\mu_0}^{\epsilon_{\max}} d\epsilon\epsilon\rho(\epsilon) - \int_{\mu_p}^{\epsilon_{\max}} d\epsilon\epsilon\rho(\epsilon), \qquad (35)$$

which should be negative if ferromagnetism is stable. The chemical potentials, μ_0 and μ_p, correspond to the unpolarized and fully polarized systems, respectively and $\epsilon_{\max}$ is the energy at the upper edge of the band. Inserting $\rho(\epsilon)$ for $t>0$ in expression (35) with $n=1.3$ we obtain $\Delta E=0.603|t|$, to be compared with $\Delta E=1.34|t|$ for $t<0$. Interestingly, for the square lattice, $\Delta E=0.8|t|$, which is between the values of ΔE for the $t<0$ and $t>0$ triangular lattices. Hence, although unsurprisingly ferromagnetism is not stable for the noninteracting system regardless of the sign of t, the ferromagnetic tendencies are clearly stronger in the electron doped triangular lattice for $t>0$ than they are for $t<0$ in agreement with the conclusions derived from the three site cluster analysis (Sec. II D and Fig. 2).

Finally, it is worth comparing previous studies of the t-J model on the triangular lattice with our DMFT results. A Curie-Weiss metal as well as ferromagnetism have been previously found from calculations using high temperature series expansions, for the hole doped triangular t-J model.[45] Our results for the electron doped lattice are equivalent to the hole doped case discussed in Ref. 45 once the sign of t is reversed. More specifically, ferromagnetism and Curie-Weiss metallic behavior appear in the high temperature expansion for the hole doped system with $t<0$ while a weak temperature dependent susceptibility appears when $t>0$. Furthermore, a heavy fermion state, analogous to our strongly correlated metallic state for $t>0$, is predicted to exist in the hole doped system with $t<0$. The qualitative agreement of the magnetic response obtained from DMFT compared with the high temperature studies (which includes both local and nonlocal correlation effects) of the t-J model indicate the importance of the local aspects of electronic correlations. This has also been pointed out in the context of metallic magnetism for which a good a description of the electronic and magnetic properties of Fe and Ni is attained from a local theory such as DMFT.[74]

VII. COMPARISON WITH EXPERIMENTS ON Na_xCoO_2

As this work has been largely motivated by experiments on Na_xCoO_2 we now consider what the lessons learned from a DMFT study of the Hubbard model on a triangular lattice might have to say about Na_xCoO_2. First, our results show that the details of the electronic structure, and in particular the DOS, play a crucial role in determining the physics of strongly correlated frustrated systems such as Na_xCoO_2. This is something of a pyrrhic victory in that this very result tells us that there is little hope of quantitative agreement between experiments on Na_xCoO_2 and calculations based on a simplified one band models with nearest neighbor hopping only, such as those presented above. Indeed our results do not show any such quantitative agreement.

In particular for the triangular lattice with $t<0$ (which, of the two cases we considered, gives the band structure closest to those suggested by both ARPES and LDA-DFT) the DMFT of the electron doped Hubbard model closely resembles a weakly interacting metal. This is clearly not what is observed in Na_xCoO_2, even at a qualitative level.

On the other hand many of the results for $t>0$ are qualitatively consistent with the picture drawn by experiments on Na_xCoO_2. In particular we propose that the experimental "Curie-Weiss metal" is little more than the "bad metal" in the extreme situation of very strong electronic correlations and high frustration. Important experimental support for this hypothesis comes from the fact that a Fermi liquidlike resistivity has only been observed[18] when $T\lesssim 1$ K which suggests that $T^*\sim 1$ K. An obvious objection, that T^* predicted by DMFT will not be this small for any reasonable parameters, will be discussed below (Sec. VIII A 1).

Our results for $t>0$ show that magnetism is a genuinely quantum many-body effect, in particular the magnetism has little resemblance to simple Stoner ferromagnetism. We propose that the observed A-type antiferromagnetism results from in plane Nagaoka ferromagnetism with a weak interlayer antiferromagnetic coupling. The observation[14,15] that the strength of the effective in-plane ferromagnetic coupling in Na_xCoO_2 is the same order of magnitude as the effective interlayer antiferromagnetic interaction despite the highly two-dimensional crystal and band structures of Na_xCoO_2 is naturally explained in this scenario as the effective ferromagnetic interaction in the Nagaoka is much weaker than the intrinsic antiferromagnetic interaction which gives rise to the phase. This can be seen from Fig. 10, here $\theta(n)$ becomes positive and ferromagnetism is suppressed by reducing the doping towards the critical doping which is the lower bound for which ferromagnetism is observed. The intrinsic antifer-

romagnetic interactions due to superexchange are given by $J=4t^2/U=0.4|t|$ for $U=10|t|$, which we take in the calculations above. Therefore even though $J=4t^2/U \gg J_\perp=4t_\perp^2/U$, where $J_\perp$ and $t_\perp$ are, respectively, the interplane exchange constant and hopping integral, near the phase transition to ferromagnetism $J \gg \theta(n)$ and thus the interplane antiferromagnetic exchange may be the same order of magnitude as the in-plane ferromagnetic exchange, as is observed experimentally in Na_xCoO_2.

To qualitatively test these ideas calculations with a more realistic band structure are required. LDA calculations predict that the dispersion of the bands is rather different to the dispersion obtained from a nearest-neighbor isotropic triangular lattice. In particular the LDA band is much flatter close to the Γ point. Indeed this is just the sort of change that is likely to have a significant effect on the results of the type of calculations we have presented above. In the current work we have also neglected the possibility of Fermi surface pockets near the K points arising from the e'_{2g} band.[47,48] Recall that, for example, we demonstrated that the magnetism and Curie-Weiss metal behavior we observed in the triangular lattice depend crucially on the DOS *near* to the Fermi level and not just on the DOS *at* the Fermi energy. Therefore, even if this band does not actually cross the Fermi energy, as some studies have indicated,[46,51] it may play an important role in Na_xCoO_2. Interestingly, the e'_{2g} band can be fitted to a $t>0$ tight-binding model close to the Fermi energy. Hence, the e'_{2g} bands may play an important role in producing the Curie-Weiss metallic state. Anyway, the generalization of these results to multiband systems[52] is likely to be important for a complete understanding on the magnetic and transport properties of Na_xCoO_2.

To quantify these remarks we now present a comparison of the DMFT results for the triangular lattice with the experimentally measured properties of Na_xCoO_2.

A. Electronic heat capacity

The experimental[77,78] value of the linear T coefficient of the specific heat ($C_v \approx \gamma T$ for $T<T^*$ with $T^*=1$ K) in Na_xCoO_2 and $0.7<x<0.82$ is $\gamma=25-30$ mJ/(mol K^2) in zero magnetic field. This corresponds to an effective mass enhancement $m^*/m_b \approx 3-4$ where m_b is the LDA band mass. On applying an external magnetic field of $H=14$ T, γ is suppressed leading to $\gamma=0.02$ J/(mol K^2) (Ref. 77) implying at 20–30% a decrease in m^*. The observed temperature and magnetic field dependence also has two unusual features. In zero field, $C_v(T)/T$ is nonmonotonic, but becomes monotonic in a field of 14 T (see Fig. 3 in Ref. 77). The reduction of $C_v(T)/T$ as the temperature increases from 1 to 5 K is consistent with the destruction of quasiparticles in this temperature range (compare Fig. 37 in Ref. 20)

Our DMFT calculations for $n=1.7$ and $U=10|t|$, predict a weak renormalization of the electrons, $m^*/m_b \approx 1.1$, for $t<0$ and $m^*/m \approx 1.5$ for $t>0$. However, in the discussion to follow it will be important to note that as the system is driven towards half filling, $n \to 1$, we find effective mass enhancements which are comparable to or larger than experimental values (see Fig. 10). Note that effective mass enhancement for $t<0$ is rapidly suppressed (Fig. 10) as n is increased above $n>1.2$ becoming effectively a weakly correlated metal for this doping region. But, for $t>0$ we find that the mass enhancement remains large to much higher dopings than for $t<0$ (for $t>0$ the mass enhancement is comparable or greater than that observed experimentally for $x \lesssim 1.5$).

B. Low-temperature resistivity

Experimentally,[18] the resistivity varies as, $\rho(T) \approx \rho_0 + AT^2$, as is expected for Fermi liquid, below $T \approx 1$ K. The coefficient of the quadratic term is measured[18] to be $A=0.96$ $\mu\Omega$ cm/K^2 for $Na_{0.7}CoO_2$. On applying an external magnetic field up to $H=16$ T, the quadratic coefficient of resistivity is decreased to $A=0.22$ $\mu\Omega$ cm/K^2 and T^* is increased to 4 K.

DMFT predicts Fermi liquid behavior below T^*, the low energy coherence scale. The resistivity coefficient predicted by DMFT is $A=0.0053$ $\mu\Omega$ cm/K^2 for $t<0$, $n=1.7$ and $U=10|t|$, which is more than two orders of magnitude smaller than the experimental value. However, at half-filling and $U=10|t|$, $A=0.81$ $\mu\Omega$ cm/K^2, which is comparable to the experimental result. For $t>0$, $n=1.7$ and $U=10|t|$ we find $A=0.32$ $\mu\Omega$ cm/K^2, which is the same order of magnitude as in experiments of Na_xCoO_2. Therefore, either the details of the DOS or driving the system towards the Mott transition could be responsible for the large value of A observed experimentally. However it is important to stress that in our calculations the coherence scale, $T^* \approx 100$ K for $U=10|t|$ at half-filling, is two orders of magnitude larger than the temperature below which $\rho(T) \approx \rho_0 + AT^2$ in the experiments.[18] We will discuss the reasons for this below (see Sec. VIII A 1).

C. Kadowaki-Woods ratio

The Kadowaki-Woods ratio of $Na_{0.7}CoO_x$ is experimentally found[18] to be $A/\gamma^2=60a_0$, with $a_0=10^{-5}$ $\mu\Omega$ cm mol^2 K^2/mJ^2 being the constant value found in the heavy-fermion materials. The large values of the ratio have been recently discussed by Hussey,[19] who explained that when volumetric rather than molar quantities for the specific heat, the values of A/γ^2 are comparable to the ones in the heavy fermion systems. From the DMFT calculations with $t<0$ we find that $A/\gamma^2=64.2a_0$ for $n=1.7$ whereas at half-filling $A/\gamma^2=75a_0$, implying a weak dependence with the electron doping. A stronger dependence is found from DMFT for $t>0$ for which the ratios vary between $A/\gamma^2=100a_0$ for $n=1.7$ and $170a_0$ at half-filling (see Fig. 13). Thus, the absolute values depend strongly on the DOS.

D. Uniform magnetic susceptibility

Experimentally, the magnetic susceptibility is found to have a Curie-Weiss form, $\chi(T) \sim 1/(T+\theta)$, and a magnitude much larger than the Pauli susceptibility expected for weakly interacting metal across a large range of dopings that have metallic ground states.[8,11] Our DMFT calculations for $t<0$ display Pauli paramagnetism, which is typical of weakly cor-

related metals, in qualitative disagreement with experiments. However, for $t>0$ a Curie-Weiss metal is observed across a wide range of dopings. In the discussion that follows it will be important to recall that the DMFT prediction of the susceptibility of a metal close to the Mott transition is that it has the Curie-Weiss form with $\theta=T^*+J>0$. Thus, a behavior similar to the experimentally observed Curie-Weiss metal is predicted by DMFT for $t>0$ [i.e., when $\rho(\epsilon_F)$ is large] and near to the Mott transition.

E. Sommerfeld-Wilson ratio

The experimentally measured Sommerfeld-Wilson ratio[79] of $Na_{0.7}CoO_2$ is $R_W=\lim_{T\to 0}(\chi(T)/\chi_0)/(\gamma/\gamma_0)=7.8$. For the hypercubic lattice, the Wilson ratio predicted by DMFT goes to zero close to the Mott transition, i.e., at half-filling, but becomes finite as soon as the system is doped away from half-filling.[20] On the triangular lattice with $t<0$ we find that the Wilson ratio attains its largest values at $n=1.6$ at which $R_W=1.7$ and decreases to 1.3 as $n\to 2$ with $U=10|t|$. In the limit $n\to 1$, the calculated $R_W=0.8$. On the other hand for $t>0$, R_W becomes extremely large at dopings close to the ferromagnetic instability. For example, for $n\approx 1.65$, R_W is already about 6. One should note that experimentally, $x=0.7$ is extremely close to the critical doping at which the A-type antiferromagnetism appears. Therefore the large Sommerfeld-Wilson ratio observed is probably a direct consequence of the proximity of $Na_{0.7}CoO_2$ to the magnetic transition. This analysis would also suggest that as the doping is decreased from $x=0.7$ then R_W will also decrease, although calculations with a more realistic band structure are required to confirm that DMFT makes this prediction.

F. Effect of a small external magnetic field on the low-T resistivity, A, and specific heat, γ, coefficients

A rapid suppression of the low-T resistivity coefficient A and specific heat slope γ and an increase in T^* are observed when an external small magnetic field is applied to Na_xCoO_2. [The details of the experimental observations of the behavior of γ (Ref. 77) and A (Ref. 18) are summarized in Secs. VII A and VII B, respectively.]

For the single impurity Kondo model the temperature dependence of the heat capacity has a maximum near the Kondo temperature. In a magnetic field, once the Zeeman energy, $g\mu_B B$, is comparable to the Kondo energy, $k_B T_K$, this maximum shifts to higher temperatures.[80,81] Based on this we would expect that the coherence temperature becomes larger with increasing field.

DMFT for the Hubbard model in a magnetic field shows that in the metallic phase of a weakly interacting metal the quasiparticle weight Z increases with field, consistent with the predictions of Stoner theory (see Fig. 5 of Ref. 58). Consequently, the specific heat coefficent γ will decrease with field. Similarily, the resistivity coefficient A will also decrease. In contrast, a strongly correlated metal close to the Mott transition displays a weak suppression with magnetic field (see inset of Fig. 9 in Ref. 58).

G. Failure of one band models with nearest neighbor hopping

The disagreements highlighted above between the one band model with nearest neighbor hopping and experiments on Na_xCoO_2, particularly for $t<0$ which is the appropriate sign of t for Na_xCoO_2, does not appear to be a result of the DFMT approximation. Our results are entirely consistent with the series expansions[45] and RVB (Ref. 23) results for the $t-J$ model on a triangular lattice in this regard. Therefore we believe that simple one band models with nearest neighbor hopping cannot only account for the observed behavior of Na_xCoO_2. This is an extremely important result given the number of theoretical papers on both Na_xCoO_2 and $Na_xCoO_2\cdot yH_2O$ that are based on this type of model. In the next section we examine what kind of models or approximations are required to give an account of the strong correlation effects in Na_xCoO_2.

VIII. MORE REALISTIC MODELS OF Na_xCoO_2

A. Beyond DMFT

Although DMFT calculations on the triangular lattice suggest the proximity of the metal to a Mott insulating phase several aspects of the observed low temperature behavior of Na_xCoO_2 are still difficult to understand. Foremost among these is why is the value of T^* estimated from resistivity so much smaller than the obtained from the susceptibility and DMFT?

The experimental value for the coherence temperature, $T^*=1$ K, as determined from the temperature below which $\rho(T)=\rho_0+AT^2$, is two orders of magnitude smaller than the DMFT result, $T^*\approx 0.1|t|\approx 100$ K for $U=10|t|$ at half-filling. For $t>0$ there is only a weak increase in T^* with doping (see Fig. 5). Driving the system closer to the Mott transition by increasing U would lead to a strong suppression of T^*, e.g., $T^*\to 0$ as $U\to U_c$ at half-filling. On the other hand, the values of T^* predicted by DMFT are comparable with values of $\theta\approx 150$ K found experimentally[8] from the Curie-Weiss fit of the spin susceptibility, $\chi(T)\approx 1/(T+\theta)$, at large temperatures.

Spin susceptibility experiments on Na_xCoO_2 show a clear departure from the simple high temperature Curie-Weiss susceptibility at temperatures of order the coherence temperature predicted by DMFT (but orders of magnitude above the temperature where the resistivity is observed to vary quadratically with temperature). Below this temperature the spin susceptibility is strongly enhanced in contrast to the DMFT prediction of a Pauli susceptibility below T^*. Although on this front one should beware of the major differences[12] between the susceptibilities measured by Foo *et al.*[8] and those measured by Prabhakaran *et al.*[11]

Spin fluctuations: All of the results presented in this paper were obtained from a purely local theory, DMFT. Therefore these results neglect short range ferromagnetic fluctuations which are likely to become increasingly important as one dopes towards the ferromagnetic phase. Indeed such ferromagnetic fluctuations have already been observed by neutron scattering in $Na_{0.7}CoO_2$.[13–15]

The importance of these fluctuations can be addressed within Moriya's[82] spin fluctuation theory of the electronic

and magnetic properties of nearly ferromagnetic metals. The theory assumes that the dynamic spin susceptibility has the form

$$\chi(\mathbf{q},\omega) = \frac{\chi(\mathbf{q}=\mathbf{0},\omega=0)}{1+\xi^2\left(q^2 - \frac{i\omega}{\Gamma q}\right)} \tag{36}$$

in two dimensions. ξ is the ferromagnetic correlation length and Γ is a phenomenological parameter. This has the same frequency and wave vector dependence as one obtains from a RPA treatment of a Fermi liquid metal.

Within this framework, the electronic properties can be sensitive to an applied magnetic field as, at low temperatures, it suppresses the ferromagnetic fluctuations, driving the system into an unrenormalized Fermi liquid state. The low temperature scale T_0 is defined by[82]

$$T_0 = \frac{\Gamma q_B^3}{2\pi}, \tag{37}$$

where πq_B^2 is a measure of the area of the first Brillouin zone.

The spin susceptibility is enhanced as the temperature is lowered departing from the Curie-Weiss law as a result of the enhancement of ferromagnetic fluctuations at low temperatures. Also a small magnetic field is expected to rapidly suppress A and γ as experimentally observed in Na_xCoO_2. The above arguments are consistent with evidence of strong ferromagnetic fluctuations acting in the Co planes for $x \approx 0.75$ from recent neutron scattering experiments.[13] In order to determine the importance of these spatial correlations it is desirable to compare the measurements of $\xi(q,\omega)$ in Ref. 13 with the form (36). If at a frequency ω one observes a peak of width $1/\xi$ in wave vector space, then $T_0 \sim \omega(q_B\xi)^3$. One sees from Figs. 1 and 4 in Ref. 13 that for $\omega \simeq 10$ meV that $q_B\xi \sim 0.4$. Hence, $T_0 \sim 1-10$ K and so the ferromagnetic fluctuations could be the origin of the low energy scale in Na_xCoO_2.

B. Beyond the single band Hubbard model

1. Role of ordering of the sodium ions

We believe that the A-type antiferromagnetic phase observed experimentally corresponds to the ferromagnetic phase predicted by DMFT and many of the metallic state properties can be interpreted in terms of their proximity to a ferromagnetic transition and strong Coulomb repulsion effects. However, a number of experiments suggest that Na_xCoO_2 behaves like it is more strongly correlated as the doping, x, is increased. These results are difficult to understand from a simple model which only contains the Co planes as such models become more weakly correlated as the electronic doping is increased due to the small number of holes left in the Co planes. Below we propose that the ordering of the Na atoms observed at many dopings provides a natural explanation of these effects as it can effectively drive the system towards half filling by introducing a spatial modulation of the site energy of the Co atoms. The suggestion that Na ordering plays a crucial role that has not been appreciated until now is made more plausible by the very sensitive dependence of the magnetic and transport properties on the exact details of the DOS that we have demonstrated above.

It seems likely that the charge ordering of the electrons in the CoO_2 layers observed at $x=0.5$ is induced by Na ordering.[8] Recently, experimental studies by Zandbergen *et al.*[83] and Roger *et al.*,[84] first principles calculations by Zhang *et al.*[85] and classical electrostatic calculations by Zhang *et al.* and Roger *et al.* have shown that as x is varied not only is the doping of the CoO_2 planes varied, but so is the Na ordering. However, there remains debate over the exact nature of the Na order at specific values of x.[83–85] There is additional evidence from NMR experiments of the presence of inequivalently charged Co ions with Co^{3+} ($S=0$) and Co^{4+} ($S=1/2$) induced by the charged Na layer of ions.[79] This effect implies that a large fraction of the electrons in the Co planes behave as $S=1/2$ localized moments. This is precisely the behavior expected close to the Mott insulating phase in a Hubbard model close to half-filling as described by DMFT.

To make this proposal more concrete we analyze four special cases, $x=0.33$, 0.5, 0.71, and 0.75. For each of these we take the orderings proposed by Zhang *et al.*[85] and Zandbergen *et al.*[83] although we note that in two of these cases ($x=0.71$ and 0.75) Roger *et al.* have proposed different Na ordering patterns which involve the formation of "vacancy droplets." We stress that this work has nothing to contribute to the debate over which patterns are, in fact, realized and we take these patterns at $x=0.71$ and 0.75 merely to exemplify our point. In the cases of $x=0.33$ and 0.5 we find that the Na ordering introduces two Co sublattices while for $x=0.71$ we find three Co sublattices and for $x=0.75$ we find four Co sublattices. For this analysis one needs to consider the two possible locations of Na in Na_xCoO_2, referred to as Na(1) and Na(2).[83] The CoO_2 planes are at $z=0.25c$, where c is the lattice constant perpendicular to the cobaltate layers. The Na(1) sites lie directly above (at $z=0.5c$) and below ($z=0$) the Co atoms, while the Na(2) sites are above or below the centres of the triangles in the triangular lattice formed by the Co atoms. The simplest model which can include the effects Na ordering is a Hubbard model which includes the Co site energy modulated by the number of nearest Na sites that are occupied. Clearly, one expects that occupied Na(1) and Na(2) will modulate the Co site energy by different amounts which we denote ε_1 and ε_2, respectively. If μ is the chemical potential for $x=0$ the Hamiltonian is then given by

$$H = \sum_{i,\sigma}(N_{1i}\varepsilon_1 + N_{2i}\varepsilon_2 - \mu)n_{i\sigma} - t\sum_{\langle ij\rangle,\sigma}(c_{i\sigma}^{\dagger}c_{j\sigma} + \text{H.c.}) + U\sum_i n_{i\uparrow}n_{i\downarrow}, \tag{38}$$

where N_{1i} and N_{2i} give the number of occupied nearest neighbor Na(1) and Na(2) sites, respectively. This model assumes that the electronic degrees of freedom relax on much shorter time scales than the Na ions move, which is reasonable because of the relative masses, even though the effective

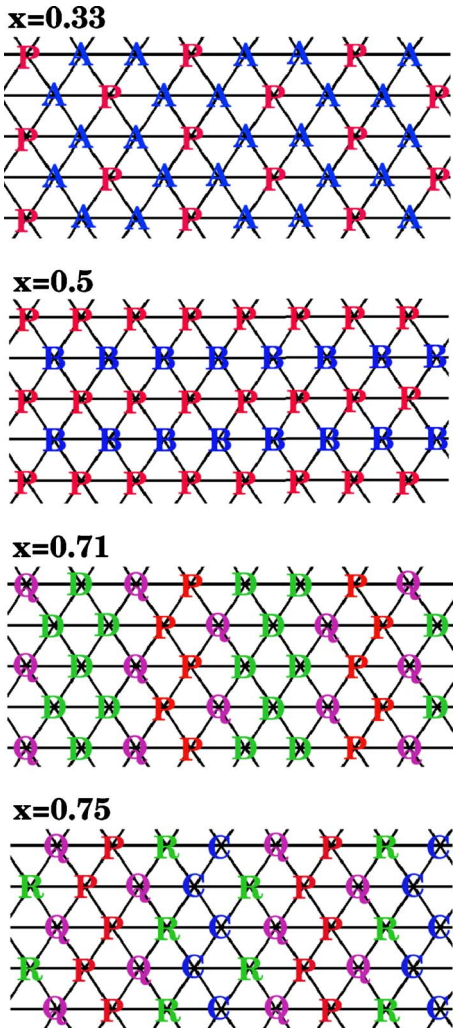

FIG. 15. (Color online) Different sublattices of cobalt ions due to commensurate ordering of sodium ions. Pictorial representation of the Hamiltonians given by Eq. (38) are shown for $x=0.33$, 0.5, 0.71, and 0.75. The different letters denote the different site energies defined by Eq. (39), so that, for example a P represents a site with site energy ε_P. These different site energies result from the different Na order patterns, which have been observed experimentally (Ref. 83) and predicted from first principles calculations (Ref. 85). The Na ordering for the quoted filling factors are taken to be those shown in Fig. 2 of Ref. 85. Note that Roger *et al.* (Ref. 84) proposed different ordering patterns for $x=0.71$ and 0.75, which involved "vacancy clustering."

quasiparticles mass is an order of magnitude larger than the bare electronic mass.

To simplify our notation we now introduce the following nomenclature:

$$\varepsilon_A = \varepsilon_2 - \mu, \quad \varepsilon_B = 2\varepsilon_2 - \mu, \quad \varepsilon_C = 3\varepsilon_2 - \mu, \quad \varepsilon_D = 4\varepsilon_2 - \mu,$$

$$\varepsilon_P = \varepsilon_1 + \varepsilon_2 - \mu, \quad \varepsilon_Q = \varepsilon_1 + 2\varepsilon_2 - \mu, \quad \varepsilon_R = \varepsilon_1 + 3\varepsilon_2 - \mu. \tag{39}$$

This allows us to sketch the relevant lattices in Fig. 15. It can be seen that for $x=0.33$ we have a honeycomb lattice of sites with site energy ε_A with the central sites in the lattice having site energy ε_P. For $x=0.5$ the lattice contains alternating chains of sites with site energy ε_B and ε_P. With $x=0.71$ we find the lattice contains sites with site energies ε_D, ε_P, and ε_Q with all three sublattices forming stripes. For $x=0.75$ a complicated arrangement of interlaced stripes of sites with site energies ε_C, ε_P, ε_Q, and ε_R is formed. This model (38) will clearly make very different predictions from the Hubbard model if the variations in the site energies caused by Na ordering are sufficiently large. For example for $x=0.5$ and $\varepsilon_P \gg \varepsilon_B$ (as one might expect) and $U \sim W$ a charge ordered insulator is likely to be the ground state of Hamiltonian (38), this is the state observed in $Na_{0.5}CoO_2$. Roger *et al.* have estimated from classical electrostatics that $\Delta\varepsilon \equiv \varepsilon_P - \varepsilon_B \simeq 100$ meV which is consistent with this scenario. Furthermore, this kind of effect will drive the system closer to Mott insulating phase if the occupation of one or more of the sublattices is strongly suppressed. Thus we expect that the DMFT treatment of (38) will have significantly better qualitative agreement with the experimentally observed properties of Na_xCoO_2 than the DMFT treatment of the Hubbard model on a triangular lattice does. Finally we note that, if one of the sublattices of $x=0.5$ can be "integrated out" of the effective low energy theory due to a large disparity in the site energies we are left with a Mott insulator on a rectangular lattice. Along one side (the horizontal direction in Fig. 15) of the rectangle it can be seen that the antiferromagnetic exchange constant is $J=4t^2/U$. In a similar manner superexchange leads to an exchange constant

$$J' = \frac{16t^4}{\Delta\varepsilon^2}\left[\frac{1}{U} + \frac{1}{2\Delta\varepsilon + U} + \frac{1}{2\Delta\varepsilon}\right] \tag{40}$$

in the perpendicular direction. Additionally there is a (diagonal) next nearest neighbor exchange interaction

$$J'' = \frac{4t^4}{\Delta\varepsilon^2}\left[\frac{1}{U} + \frac{2}{2\Delta\varepsilon + U}\right]. \tag{41}$$

It is interesting to consider the three limiting cases:

$$\text{for } U \gg \Delta\varepsilon, \quad \frac{J'}{J} = \frac{2t^2U}{(\Delta\varepsilon)^3} \quad \text{and} \quad \frac{J''}{J'} = \frac{3\Delta\varepsilon}{2U} \ll 1;$$

$$\text{for } U \ll \Delta\varepsilon, \quad \frac{J'}{J} = \frac{4t^2}{(\Delta\varepsilon)^2} \ll 1 \quad \text{and} \quad \frac{J''}{J'} = 4;$$

$$\text{for } U = \Delta\varepsilon, \quad \frac{J'}{J} = \frac{6t^2}{U^2} \ll 1 \quad \text{and} \quad \frac{J''}{J'} = \frac{5}{18}.$$

In particular note that for $U \gg \Delta\varepsilon$ we may have $J' \sim J$. Neutron scattering experiments suggest that the charge ordered phase of $Na_{0.5}CoO_2$ has long range Néel order[86] which suggests $J \sim J' > J''$ and is therefore consistent with this model when $U \gg \Delta\varepsilon \gg t$, which is precisely the regime that the separate estimates of these three parameters suggest we are in.

Before moving on from the effects of Na ordering it is interesting to note that this type of problem is actually rather general in doped systems. For example, in most models of the cuprates it is assumed that the only effect of varying the

doping is to vary the electronic density in the CoO_2 layers. However, if it is confirmed that Na ordering plays the role we have proposed in Na_xCoO_2 then this may be an important step towards a general understanding of the role of dopant impurities in strongly correlated systems.

We stress that the above proposal relies on Na ordering and not disorder. It is well known that disorder only plays a significant role in DMFT when there are rather extreme levels of disorder.[87] Therefore one would not expect our results to be significantly affected by the low levels of disorder typically found in Na_xCoO_2. However, recently the role of disorder on the band structure of Na_xCoO_2 has received some attention.[88] If disorder does induce significant changes in the DOS this would be an important factor for the results reported in this paper. More generally, the role of disorder in $Na_xCoO_2 \cdot yH_2O$ will no doubt prove an important probe of whether the superconducting state is conventional or not.[89]

2. Multiple bands

The model, as written in Eq. (38), only contains a single band. As discussed in the above band structure calculations suggest a simple one band model is not sufficient to describe the band structure of Na_xCoO_2. Although the a_{1g} band can be roughly fitted to a tight-binding model with $t<0$ which is consistent with the large hole pocket around the Γ point, additional small hole pockets may be present in the Fermi surface associated with the e'_{2g} bands crossing the Fermi energy. These bands can be fitted to a $t>0$ tight-binding band which is likely to favor ferromagnetism. Such a multiband model is a straightforward generalization of (38) giving

$$H = \sum_{i\sigma\nu} (N_{1i\nu}\varepsilon_1 + N_{2i\nu}\varepsilon_2 - \mu_\nu) n_{i\nu\sigma} - \sum_{ij\nu\nu'\sigma} t_{ij\nu\nu'} (c^\dagger_{i\nu\sigma} c_{j\nu'\sigma} + \text{H.c.}) + \sum_{i\nu\nu'} U_{\nu\nu'} n_{i\nu\sigma} n_{i\nu'\sigma'}, \tag{42}$$

where the labels ν and ν' refer the different orbitals. A multiband DMFT treatment is likely to describe both of the following effects: (i) the proximity of the metal to a Mott insulating phase leading to renormalized quasiparticles and Curie-Weiss behavior for $T>T^*$ and (ii) the strong ferromagnetic fluctuations appearing at very low temperatures. Several models have been recently proposed to describe Na_xCoO_2. In comparison to single band[23,36] and multiband Hubbard models,[48,49,52] our proposed model explicitly contains the periodic potential of the Na layers acting on the Co planes in combination with the Coulomb interaction. This is an important ingredient to understand the unexpected Curie-Weiss susceptibility and large effective mass at $x \to 0.7$. At these large dopings the system is expected to behave as a weakly correlated metal. We believe that our model is sufficient to fully understand the interplay between these two essential ingredients of the problem.

The problem of applying DMFT to a Hubbard model with two inequivalent sublattices has been considered before. Chitra and Kotliar[90] considered the Hubbard model at half filling in the presence of antiferromagnetic order. This leads to a different chemical potential on the two sublattices. Bulla and co-workers[91] considered charge ordering in the extended Hubbard model at one-quarter filling. For the case of the Bethe lattice the model was mapped to a pair of Anderson impurity models, one for each of the two sublattices. For V (the Coulomb repulsion between electrons on neighboring lattice sites) larger than about t and $U=2t$ the quasiparticle weight (and presumably the coherence temperature also) is orders of magnitude smaller than the noninteracting value and there is a pseudogap in the density of states. Based on the above we would expect that for $x=0.5$ the ground state will be an insulator if $|\varepsilon_P - \varepsilon_B| \sim U > |t|$ due to the two different sublattices.

IX. CONCLUSIONS

We have presented a DMFT analysis of the electronic and magnetic properties of the doped isotropic triangular Hubbard model. An important result of our work is the large effect of the bare DOS on its magnetic and electronic properties. In particular, a Curie-Weiss metal is found for $t>0$ and $U \gtrsim W$. In contrast, Pauli paramagnetism is found for $t<0$ regardless of the magnitude of U. We find a larger degree of localization and a larger renormalization of the electrons for $t>0$ than for $t<0$ due to the different DOS at the Fermi energy. The spin susceptibility crosses over from Curie-Weiss behavior, at large temperatures, to a renormalized Fermi liquid as $T \to 0$. At low temperatures, the uniform spin susceptibility is strongly enhanced for $t>0$ due to the proximity to the ferromagnetic transition. This is in contrast to the behavior for $t<0$, for which only a small enhancement of $\chi(T \to 0)/\chi_0$ is found. The stronger renormalization of the quasiparticles found for $t>0$ than for $t<0$ when the system is doped away from half-filling is a consequence of a larger DOS near the Fermi energy in the $t>0$ case.

For $t>0$ we find a metallic ferromagnetic state when U is sufficiently large. The ferromagnetism is significantly different from Stoner ferromagnetism in that it has a strong local moment character and the criterion for ferromagnetism is not simply related to the DOS at the Fermi level, but depends on the features of the DOS over a significant energy range around the Fermi level. No ferromagnetism has been found for any band filling or any value of U when $t<0$, which is qualitatively different from the prediction of Stoner theory. We conclude that the ferromagnetism we have observed is much more closely related to Nagaoka ferromagnetism. The different behavior of the two lattices is due to kinetic energy frustration which dramatically reduces the energy cost of polarizing the system for $t>0$. We have therefore proposed that the A-type antiferromagnetic phase observed in Na_xCoO_2 for $x>0.75$ is the result of in plane Nagaoka-type ferromagnetism.

The different behaviors encountered away from half-filling for the different signs of t contrasts with the system sufficiently close to the Mott insulating phase ($n \to 1$ and $U > U_c$ or $U \to U_c$ and $n=1$). In this case, the model displays very similar properties including Curie-Weiss susceptibility with $\theta>0$ (due to antiferromagnetic superexchange interaction close to half-filling), a large effective mass enhancement, ($m^*/m_b=5$ for $U=10|t|$), large low-T resistivity coef-

ficient, and enhanced Kadowaki-Woods ratio.

Thus our results show that the details of the band structure are extremely important for understanding the metallic and spin ordered phases of Na_xCoO_2. In particular, a simple one-band Hubbard model on a triangular lattice is not enough to understand the unconventional properties of Na_xCoO_2. Our results however do suggest that the Curie-Weiss susceptibility observed in the metallic phase of Na_xCoO_2 results from incoherent quasilocalized electrons. Remarkably, the DMFT estimate of $T^*=0.1|t|\approx 100-200$ K is in good agreement with the Curie-Weiss constant $\theta\approx 150$ K experimentally measured.

Many of the thermodynamic and transport properties observed in Na_xCoO_2, for large x, are consistent with the DMFT prediction of the transport and magnetic properties of the metal very close to the Mott transition. We have proposed that Mott physics is relevant to Na_xCoO_2 even when x is large and the system is far away from the Mott insulating phase because of experimental observation of charge ordering in the Co planes.

The T dependence of several transport and magnetic properties is consistent with the DMFT description of a metal close to the Mott transition for $T>T^*$. However, at very low temperatures, experimental observations on Na_xCoO_2, depart from our DMFT results. For instance, the susceptibility deviates significantly from the Curie-Weiss behavior being strongly enhanced below $T\sim 80$ K. Also transport and thermodynamic quantities are very sensitive to a small applied magnetic field. One is tempted to associate the very low temperature scale of about 1 K experimentally determined to the DMFT coherence scale, T^*, which goes to 0 as the system approaches the Mott insulating state. However, such a small value of T^* implies an extremely large effective mass enhancement in clear disagreement with experimental values, $m^*/m_b\sim 3-4$. We conclude that this very small energy scale is due to low energy ferromagnetic fluctuations in the Co planes which are neglected within the DMFT. These fluctuations would scatter the strongly renormalized quasiparticles which are properly described by DMFT.

We have then used this analysis to help identify the simplest relevant model that captures the essential physics in Na_xCoO_2. We have proposed a model which contains the charge ordering phenomena observed in the system that we have proposed drive the system close to the Mott insulating phase for the large dopings. Band structure calculations find that the a_{1g} band can be roughly fitted to a tight-binding model with $t<0$ which roughly describes the large hole pocket around the Γ point. Additional small hole pockets may be present in the Fermi surface associated with the e'_{2g} bands crossing the Fermi energy. These bands can be fitted to a $t>0$ tight-binding band for which ferromagnetic fluctuations are likely to exist. Hence, a multiband DMFT treatment containing the a_{1g} and e'_{2g} bands as well as charge ordering phenomena should describe both the following aspects: (i) the proximity of the metal to a Mott insulating phase leading to renormalized quasiparticles and Curie-Weiss behavior for $T>T^*$ and (ii) the strong ferromagnetic fluctuations appearing at low temperatures. We believe that a model including both of these ingredients is needed to fully understand the physics of Na_xCoO_2.

ACKNOWLEDGMENTS

It is a pleasure to acknowledge helpful discussions with A. Boothroyd, R. Coldea, J. O. Fjærestad, C. Hooley, M. D. Johannes, A. Levy-Yeyati, B. Lake, M. Long, S. Nagler, F. Rivadulla, A. J. Schofield, D. J. Singh, and D. A. Tennant. We thank the Clarendon Laboratory, Oxford University and the Rutherford Appleton Laboratory for hospitality. J.M. is grateful to the Ramón y Cajal program from Ministerio de Ciencia y Tecnología in Spain and EU through Contract No. MERG-CT-2004-506177 for financial support. B.J.P. and R.H.M. were supported by the Australian Research Council. Some of the calculations were performed at the Scientific Computational Center of Universidad Autónoma de Madrid.

[1] See, for example, N. P. Ong and R. J. Cava, Science **305**, 52 (2004).

[2] BEDT-TTF is *bis*(ethylenedithio)-tetrathiafulvalene.

[3] For $X\in\{Me_4Z, Et_2Me_2Z\}$ and $Z\in\{P, Sb\}$ where Me=CH_4, Et=C_2H_5 and dmit=1,3-dithiol-2-thione-4,5-dithiolate.

[4] Y. Shimizu, K. Miyagawa, K. Kanoda, M. Maesato, and G. Saito, Phys. Rev. Lett. **91**, 107001 (2003).

[5] M. Tamura and R. Kato, J. Phys.: Condens. Matter **14**, L729 (2002); R. Kato, Chem. Rev. (Washington, D.C.) **104**, 5319 (2004).

[6] R. Coldea, D. A. Tennant, and Z. Tylczynski, Phys. Rev. B **68**, 134424 (2003).

[7] S. Nakatsuji, Y. Nambu, H. Tonomura, O. Sakai, S. Jonas, C. Broholm, H. Tsunetsugu, Y. Qiu, and Y. Maeno, Science **309**, 1697 (2005).

[8] M. L. Foo, Y. Wang, S. Watauchi, H. W. Zandbergen, T. He, R. J. Cava, and N. P. Ong, Phys. Rev. Lett. **92**, 247001 (2004).

[9] J. Sugiyama, J. H. Brewer, E. J. Ansaldo, H. Itahara, T. Tani, M. Mikami, Y. Mori, T. Sasaki, S. Hébert, and A. Maignan, Phys. Rev. Lett. **92**, 017602 (2004).

[10] Y. Wang, N. S. Rogado, R. J. Cava, and N. P. Ong, Nature (London) **423**, 425 (2003).

[11] D. Prabhakaran, A. T. Boothroyd, R. Coldea, L. M. Helme, and D. A. Tennant, cond-mat/0312493 (unpublished).

[12] Foo *et al.* (Ref. 8) measured the susceptibility in 5 T on a single crystal with the field aligned to the c axis whereas Prabhakaran *et al.* (Ref. 11) used only 100 Oe and studied polycrystalline samples.

[13] B. G. Elmegreen, L. Krusin-Elbaum, T. Shibauchi, and B. Argyle, Phys. Rev. Lett. **93**, 197201 (2004).

[14] S. P. Bayrakci, I. Mirebeau, P. Bourges, Y. Sidis, M. Enderle, J. Mesot, D. P. Chen, C. T. Lin, and B. Keimer, Phys. Rev. Lett. **94**, 157205 (2005).

[15] L. M. Helme, A. T. Boothroyd, R. Coldea, D. Prabhakaran, D. A. Tennant, A. Hiess, and J. Kulda, Phys. Rev. Lett. **94**, 157206 (2005).

[16] J. Sugiyama, J. H. Brewer, E. J. Ansaldo, H. Itahara, T. Tani, M. Mikami, Y. Mori, T. Sasaki, S. Hébert, and A. Maignan, Phys. Rev. Lett. **92**, 017602 (2004).
[17] Y. Nagaoka, Phys. Rev. **147**, 392 (1966).
[18] S. Y. Li, L. Taillefer, D. G. Hawthorn, M. A. Tanatar, J. Paglione, M. Sutherland, R. W. Hill, C. H. Wang, and X. H. Chen, Phys. Rev. Lett. **93**, 056401 (2004).
[19] N. E. Hussey, J. Phys. Soc. Jpn. **74**, 1107 (2005).
[20] For a review see, A. Georges, G. Kotliar, W. Krauth, and M. J. Rozenberg, Rev. Mod. Phys. **68**, 13 (1996).
[21] Th. Pruschke, M. Jarrell, and J. K. Freericks, Adv. Phys. **44**, 187 (1995).
[22] J. Merino and R. H. McKenzie, Phys. Rev. B **61**, 7996 (2000).
[23] B. Kumar and B. S. Shastry, Phys. Rev. B **68**, 104508 (2003).
[24] B. Bernu, P. Lecheminant, C. Lhuillier, and L. Pierre, Phys. Rev. B **50**, 10048 (1994).
[25] L. Capriotti, A. E. Trumper, and S. Sorella, Phys. Rev. Lett. **82**, 3899 (1999).
[26] D. A. Huse and V. Elser, Phys. Rev. Lett. **60**, 2531 (1988).
[27] D. J. J. Farnell, R. F. Bishop and K. A. Gernoth, Phys. Rev. B **63**, 220402(R) (2001).
[28] R. R. P. Singh and D. A. Huse, Phys. Rev. Lett. **68**, 1766 (1992).
[29] Weihong Zheng, R. H. McKenzie, and R. P. Singh, Phys. Rev. B **59**, 14367 (1999).
[30] A. V. Chubukov, S. Sachdev, and T. Senthil, J. Phys.: Condens. Matter **6**, 8891 (1994).
[31] See, for example, Sec. II, of Ref. 62 for a more extensive discussion and the background references.
[32] M. Capone, L. Capriotti, F. Becca, and S. Caprara, Phys. Rev. B **63**, 085104 (2001).
[33] B. J. Powell and R. H. McKenzie, Phys. Rev. Lett. **94**, 047004 (2005).
[34] A. H. MacDonald, S. M. Girvin, and D. Yoshioka, Phys. Rev. B **41**, 2565 (1990); **37**, 9753 (1988).
[35] W. LiMing, G. Misguich, P. Sindzingre, and C. Lhuillier, Phys. Rev. B **62**, 6372 (2000).
[36] O. I. Motrunich, Phys. Rev. B **72**, 045105 (2005).
[37] S.-S. Lee and P. A. Lee, Phys. Rev. Lett. **95**, 036403 (2005).
[38] See for example, C. Weber, A. Laeuchli, F. Mila, and T. Giamarchi, Phys. Rev. B **73**, 014519 (2006).
[39] M. Vojta and E. Dagotto, Phys. Rev. B **59**, R713 (1999).
[40] M. D. Johannes, I. I. Mazin, D. J. Singh, and D. A. Papaconstantopoulos, Phys. Rev. Lett. **93**, 097005 (2004).
[41] H. R. Krishnamurthy, C. Jayaprakash, S. Sarker, and W. Wenzel, Phys. Rev. Lett. **64**, 950 (1990); C. Jayaprakash, H. R. Krishnamurthy, S. Sarker, and W. Wenzel, Europhys. Lett. **15**, 625 (1991); M. Fujita, T. Nakanishi, and K. Machida, Phys. Rev. B **45**, 2190 (1992).
[42] C. J. Gazza, A. E. Trumper, and H. A. Ceccatto, J. Phys.: Condens. Matter **6**, L625 (1994).
[43] M. Kato and F. Kokubo, Phys. Rev. B **49**, 8864 (1994).
[44] See, for example, G. Baskaran, Phys. Rev. Lett. **91**, 097003 (2003); M. Ogata, J. Phys. Soc. Jpn. **72**, 1839 (2003); C. Honerkamp, Phys. Rev. B **68**, 104510 (2003); Q.-H. Wang, D.-H. Lee, and P. A. Lee, *ibid.* **69**, 092504 (2004).
[45] T. Koretsune and M. Ogata, Phys. Rev. Lett. **89**, 116401 (2002); T. Koretsune and M. Ogata, J. Phys. Soc. Jpn. **72**, 2437 (2003).
[46] M. Z. Hasan, Y. D. Chuang, D. Qian, Y. W. Li, Y. Kong, A. P. Kuprin, A. V. Fedorov, R. Kimmerling, E. Rotenberg, K. Rossnagel, Z. Hussain, H. Koh, N. S. Rogado, M. L. Foo, and R. J. Cava, Phys. Rev. Lett. **92**, 246402 (2004); H.-B. Yang, S.-C. Wang, A. K. P. Sekharan, H. Matsui, S. Souma, T. Sato, T. Takahashi, T. Takeuchi, J. C. Campuzano, R. Jin, B. C. Sales, D. Mandrus, Z. Wang, and H. Ding, *ibid.* **92**, 246403 (2004).
[47] D. J. Singh, Phys. Rev. B **61**, 13397 (2000).
[48] K. W. Lee, J. Kunes, and W. E. Pickett, Phys. Rev. B **70**, 045104 (2004); P. Zhang, W. Luo, M. L. Cohen, and S. G. Louie, Phys. Rev. Lett. **93**, 236402 (2004).
[49] M. D. Johannes, D. A. Papaconstantopoulos, D. J. Singh, and M. J. Mehl, Europhys. Lett. **68**, 433 (2004).
[50] H. Rosner, S.-L. Drechsler, G. Fuchs, A. Handstein, A. Wälte, and K.-H. Müller, Braz. J. Phys. **33**, 718 (2003).
[51] S. Zhou, M. Gao, H. Ding, P. A. Lee, and Z. Wang, Phys. Rev. Lett. **94**, 206401 (2005).
[52] H. Ishida, M. D. Johannes, and A. Liebsch, Phys. Rev. Lett. **94**, 196401 (2005); F. Lechermann, S. Biermann, and A. Georges, Prog. Theor. Phys. Suppl. **160**, 233 (2005).
[53] R. H. McKenzie, Comments Condens. Matter Phys. **18**, 309 (1998).
[54] W. Barford and J. H. Kim, Phys. Rev. B **43**, 559 (1991).
[55] To completely define our states we must also specify the order in which they are filled. In what follows we fill the states in numerical order of site number with ↑ states for a given site filled before ↓ states. Thus we have, for example, $|\uparrow\downarrow,\uparrow\downarrow,0\rangle = c^\dagger_{2\downarrow}c^\dagger_{2\uparrow}c^\dagger_{1\downarrow}c^\dagger_{1\uparrow}|0\rangle$ and $|\uparrow\downarrow,\uparrow,\downarrow\rangle = c^\dagger_{3\downarrow}c^\dagger_{2\uparrow}c^\dagger_{1\downarrow}c^\dagger_{1\uparrow}|0\rangle$. This ensures that the singlets are negative superpositions and the triplets are positive superpositions which is intuitive. Note that this is not the case for other filling conventions, e.g., if we fill the ↑ states in numerical order and then the ↓ states in numerical order the state $c^\dagger_{3\downarrow}c^\dagger_{1\downarrow}c^\dagger_{2\uparrow}c^\dagger_{1\uparrow}|0\rangle + c^\dagger_{2\downarrow}c^\dagger_{1\downarrow}c^\dagger_{3\uparrow}c^\dagger_{1\uparrow}|0\rangle$ is a singlet.
[56] The $U\to 0$ limit of Eq. (3) is slightly confusing as one must remember that $t<0$. Using Eq. (3) we get $E(U\to 0) = (1/2)\times(-2|t| - \sqrt{36|t|^2}) - 4|t|$ as required.
[57] M. Caffarel and W. Krauth, Phys. Rev. Lett. **72**, 1545 (1994).
[58] L. Laloux, A. Georges, and W. Krauth, Phys. Rev. B **50**, 3092 (1994).
[59] P. Limelette, P. Wzietek, S. Florens, A. Georges, T. A. Costi, C. Pasquier, D. Jérome, C. Mézière, and P. Batail, Phys. Rev. Lett. **91**, 016401 (2003).
[60] A. P. Ramirez, Annu. Rev. Mater. Sci. **24**, 453 (1994).
[61] P. Schiffer and I. Daruka, Phys. Rev. B **56**, 13712 (1997).
[62] W. Zheng, R. R. P. Singh, R. H. McKenzie, and R. Coldea, Phys. Rev. B **71**, 134422 (2005).
[63] N. Elstner, R. R. P. Singh, and A. P. Young, Phys. Rev. Lett. **71**, 1629 (1993); J. Appl. Phys. **75**, 5943 (1994).
[64] Y. Imai and N. Kawakami, Phys. Rev. B **65**, 233103 (2002).
[65] M. Jarrell and J. E. Gubernatis, Phys. Rep. **269**, 133 (1996).
[66] G. Rickayzen, *Green's Functions and Condensed Matter* (Academic, London, 1980), p. 30.
[67] A. C. Hewson, *The Kondo Problem to Heavy Fermions* (Cambridge University Press, Cambridge, 1997).
[68] N. Ashcroft and D. Mermin, *Solid State Physics* (Thomson Learning, New York, 1976), p. 669.
[69] R. Fresard and K. Doll, in *The Hubbard Model: Its Physics and Mathematical Physics* (Plenum Press, New York, 1995), pp. 385–392.
[70] E. Müller-Hartmann, Z. Phys. B: Condens. Matter **74**, 507 (1989).
[71] G. Tian, J. Phys. A **23**, 2231 (1990).
[72] M. Kollar, R. Strack, and D. Vollhardt, Phys. Rev. B **53**, 9225

(1996).
[73] M. Ulmke, Eur. Phys. J. B **1**, 301 (1998).
[74] A. I. Lichtenstein, M. I. Katsnelson, and G. Kotliar, Phys. Rev. Lett. **87**, 067205 (2001); P. Pou, F. Flores, J. Ortega, R. Pérez, and A. Levy-Yeyati, J. Phys.: Condens. Matter **14**, L421 (2002).
[75] D. Vollhardt, N. Blümer, K. Held, M. Kollar, J. Schlipf, and M. Ulmke, Z. Phys. B: Condens. Matter **103**, 283 (1997).
[76] D. Vollhardt, N. Blümer, K. Held, M. Kollar, J. Schlipf, M. Ulmke, and J. Wahle, Adv. Solid State Phys. **38**, 383 (1999).
[77] M. Brühwiler, B. Batlogg, S. M. Kazakov, and J. Karpinski, cond-mat/0309311 (unpublished).
[78] T. Motohashi, R. Ueda, E. Naujalis, T. Tojo, I. Terasaki, T. Atake, M. Karppinen, and H. Yamauchi, Phys. Rev. B **67**, 064406 (2003); B. C. Sales, R. Jin, K. A. Affholter, P. Khalifah, G. M. Veith, and D. Mandrus, *ibid.* **70**, 174419 (2004); S. P. Bayrakci, C. Bernhard, D. P. Chen, B. Keimer, R. K. Kremer, P. Lemmens, C. T. Lin, C. Niedermayer, and J. Strempfer, *ibid.* **69**, 100410(R) (2004).
[79] I. R. Mukhamedshin, H. Alloul, G. Collin, and N. Blanchard, Phys. Rev. Lett. **94**, 247602 (2005).
[80] P. D. Sacramento and P. Schlottmann, Phys. Rev. B **40**, 431 (1989).
[81] See Fig. 9.12, of Ref. 67.
[82] T. Moriya, *Spin Fluctuations and Itinerant Electron Magnetism* (Springer-Verlag, Berlin, 1985).
[83] H. W. Zandbergen, M. L. Foo, Q. Xu, V. Kumar, and R. J. Cava, Phys. Rev. B **70**, 024101 (2004).
[84] M. Roger, D. J. P. Morris, D. A. Tennant, M. J. Gutmann, J. P. Goff, D. Prabhakaran, N. Shannon, B. Lake, R. Coldea, and P. P. Deen, cond-mat/0507040 (unpublished); M. Roger, D. J. P. Morris, D. A. Tennant, M. J. Gutmann, J. P. Goff, D. Prabhakaran, N. Shannon, B. Lake, A. T. Boothroyd, R. Coldea, and P. Deen, cond-mat/0510468, presented at the LT24 International Conference, Orlando, FL (2005).
[85] P. Zhang, R. B. Capaz, M. L. Cohen, and S. G. Louie, Phys. Rev. B **71**, 153102 (2005).
[86] M. Yokoi, T. Moyoshi, Y. Kobayashi, M. Soda, Y. Yasui, M. Sato, and K. Kakurai, J. Phys. Soc. Jpn. **74**, 1800 (2005); G. Gasparovic, R. A. Ott, J.-H. Cho, F. C. Chou, Y. Chu, J. W. Lynn, and Y. S. Lee, Phys. Rev. Lett. **96**, 046403 (2006).
[87] See, for example, D. Tanaskovic, V. Dobrosavljevic, E. Abrahams, and G. Kotliar, Phys. Rev. Lett. **91**, 066603 (2003), and references therein.
[88] D. J. Singh and D. Kasinathan, cond-mat/0604002 (unpublished).
[89] For a review of the effects of disorder in unconventional superconductors see, e. g., B. J. Powell and R. H. McKenzie, Phys. Rev. B **69**, 024519 (2004).
[90] R. Chitra and G. Kotliar, Phys. Rev. Lett. **83**, 2386 (1999).
[91] R. Pietig, R. Bulla, and S. Blawid, Phys. Rev. Lett. **82**, 4046 (1999); N.-H. Tong, S.-Q. Shen, and R. Bulla, Phys. Rev. B **70**, 085118 (2004).